Chapter 1
Theoretical Framework

The currently known spectrum of elementary particles consists of leptons and quarks, which constitute the different forms of matter, and vector bosons, which are the force carriers.[1] The leptons appear in three families (ν_e, e), (ν_μ, μ), (ν_τ, τ), as well as the quarks (u, d), (c, s), (t, b). In the Standard Model [1, 2], forces between these elementary fermions are due to a $SU(3) \times SU(2) \times U(1)$ gauge symmetry of the corresponding fiel theory. The $SU(2) \times U(1)$ symmetry is generating the electroweak forces, with the photon, W and Z gauge bosons. The strong force is due to the $SU(3)$ symmetry. Quantum Chromodynamics [2] (QCD) describe the interaction of quarks and the corresponding gauge bosons, the gluons. In the following, natural units, setting $c = \hbar = 1$, are chosen, and the relations $c\hbar = 197.3269631(49)$ MeV fm [3] and $c = 299{,}792{,}458\,\mathrm{ms}^{-1}$ may be used to convert between energy and space-time units.

1.1 Electroweak Interactions

The electroweak part of the Standard Model Lagrangian can be divided into three parts, a gauge boson, a fermion and a Higgs term:

$$\mathcal{L} = \mathcal{L}_G + \mathcal{L}_F + \mathcal{L}_H \tag{1.1}$$

The $SU(2)$ and $U(1)$ gauge boson field are $\mathbf{W}_\mu$ and B_μ. They couple to the weak isospin T_a and the weak hypercharge Y of the fermions. Left-handed fermion field $\psi_L = \frac{1}{2}(1 - \gamma_5)\psi$ are combined to iso-doublets. The right-handed field $\psi_R = \frac{1}{2}(1+\gamma_5)\psi$ are iso-singlets. The corresponding values of the third component of the isospin, T_3, and Y are listed in Table 1.1, together with the electric charge Q. The left-handed down-type quarks, (d', s', b'), are related to their mass eigenstates, (*d,s,b*), by the Cabibbo-Kobayashi-Maskawa (CKM) mixing matrix [4, 3] according to $d'_i = \sum_{ij} V_{ij}^{\mathrm{CKM}} d_j$.

[1] Effects of gravity are too small to be observed in the energy ranges discussed here, and are neglected.

A. Straessner, Electroweak Physics at LEP and LHC, https://10.1007/978-3-642-05169-2_1

Table 1.1 Quantum numbers of leptons and quarks. They are the eigenvalues of the third component of the weak isospin, T_3, of the weak hyper-charge, Y, and of the electrical charge, Q. The doublets of the weak isospin are put in *brackets*

Fermion Type			T_3	Y	Q
$\begin{pmatrix} \nu_e \\ e \end{pmatrix}_L$	$\begin{pmatrix} \nu_\mu \\ \mu \end{pmatrix}_L$	$\begin{pmatrix} \nu_\tau \\ \tau \end{pmatrix}_L$	$1/2$ $-1/2$	$-1/2$ $-1/2$	0 -1
$\nu_{e,R}$	$\nu_{\mu,R}$	$\nu_{\tau,R}$	0	0	0
e_R	μ_R	τ_R	0	-1	-1
$\begin{pmatrix} u \\ d' \end{pmatrix}_L$	$\begin{pmatrix} c \\ s' \end{pmatrix}_L$	$\begin{pmatrix} t \\ b' \end{pmatrix}_L$	$1/2$ $-1/2$	$1/6$ $1/6$	$2/3$ $-1/3$
u_R	c_R	t_R	0	$2/3$	$2/3$
d_R	s_R	b_R	0	$-1/3$	$-1/3$

The gauge part of the Lagrangian is given by:

$$\mathcal{L}_G = -\frac{1}{4} F_i^{\mu\nu} F^i_{\mu\nu} - \frac{1}{4} B_{\mu\nu} B^{\mu\nu} \ , \tag{1.2}$$

where $F^i_{\mu\nu}$ is the $SU(2)$ fiel strength

$$F^i_{\mu\nu} = \partial_\mu W^i_\nu - \partial_\nu W^i_\mu - g_2 \varepsilon_{ijk} W^j_\mu W^k_\nu \tag{1.3}$$

with the coupling constant g_2, and $B_{\mu\nu}$ the $U(1)$ fiel strength

$$B_{\mu\nu} = \partial_\mu B_\nu - \partial_\nu B_\mu \ . \tag{1.4}$$

The totally anti-symmetric tensor ε_{ijk} is identical to the $SU(2)$ structure constants. Due to the non-abelian $SU(2)$ group structure the W^i gauge field do not evolve independently but are coupled to each other.

The interaction between fermions and gauge bosons is most conveniently written by means of the covariant derivate

$$D_\mu = \partial_\mu + i \frac{g_1}{2} Y B_\mu + i g_2 T_a W^a_\mu \tag{1.5}$$

yielding

$$\mathcal{L}_F = \sum_f i \bar{\psi}_f D_\mu \gamma^\mu \psi_f \ , \tag{1.6}$$

where the sum extends over all fermion fields The T_a matrices are the two-dimensional representation of the group generators of the $SU(2)$, which follow the commutation relations $[T_i, T_j] = i \varepsilon_{ijk} T_k$ and $[T_i, Y] = 0$.

In the Standard Model, gauge invariant mass terms for fermions and bosons arise through the coupling to a complex doublet $\phi = \begin{pmatrix} \phi_1 \\ \phi_2 \end{pmatrix}$ of spin-zero Higgs field

and the spontaneous breaking of the $SU(2) \times U(1)$ symmetry [5]. In the minimal version there is only one Higgs doublet. The $\mathcal{L}_H$ term is completed by a dynamic term, a Higgs potential, and mass terms for the fermion fields

$$\mathcal{L}_H = D_\mu \phi^\dagger D^\mu \phi - V(\phi) + \sum_f c_f \left(\bar{\psi}_f^L \phi^\dagger \psi_f^R + \bar{\psi}_f^R \phi \psi_f^L \right) \tag{1.7}$$

The ground state $\langle \phi \rangle_0$ of the Higgs self-interaction potential

$$V(\phi) = \mu^2 \phi^\dagger \phi + \lambda (\phi^\dagger \phi)^2 \tag{1.8}$$

is found for

$$\langle \phi^\dagger \phi \rangle_0 = \frac{v^2}{2} \tag{1.9}$$

with

$$v \equiv \sqrt{\frac{-\mu^2}{\lambda}} \, . \tag{1.10}$$

The Higgs fiel is rotated so that only the lower component remains and is then developed around the vacuum expectation value:

$$\langle \phi \rangle_0 = \frac{1}{\sqrt{2}} \begin{pmatrix} 0 \\ v + H \end{pmatrix} \, . \tag{1.11}$$

This choice breaks the original $SU(2) \times U(1)$ symmetry but conserves the electric charge symmetry, $U(1)_{\mathrm{QED}}$. The energy scale v is not predicted by the model and must be measured experimentally.

With the charged vector boson field

$$W_\mu^\pm = \frac{1}{\sqrt{2}} \left(W_\mu^1 \mp i W_\mu^2 \right) \tag{1.12}$$

the particle mass terms are given by

$$\begin{aligned} \mathcal{L}_{\mathrm{mass}} = & -\frac{v}{\sqrt{2}} \sum_f c_f \bar{\psi}_f \psi_f \\ & + \left(\frac{v g_2}{2} \right)^2 W_\mu^+ W_-^\mu + \frac{v^2}{8} \left(W_\mu^3, B_\mu \right) \begin{pmatrix} g_2^2 & -g_1 g_2 \\ -g_1 g_2 & g_1^2 \end{pmatrix} \begin{pmatrix} W^{3,\mu} \\ B^\mu \end{pmatrix} \\ & + v^2 \lambda H^2 \end{aligned} \tag{1.13}$$

The Higgs boson mass depends on both v and the free parameter λ:

$$M_{\mathrm{H}} = v\sqrt{2\lambda}\ . \tag{1.14}$$

The fermion masses turn out to be

$$m_{\mathrm{f}} = \frac{v}{\sqrt{2}} c_f \tag{1.15}$$

with free Yukawa coupling constants c_f, not constrained by the model.

The measurements of neutrino fl vour oscillations [6] clearly show that neutrinos are not massless, opposed to the original version of the Standard Model [1]. In the given formalism, neutrinos can be treated in the same way as the charged leptons. Like for quarks, the neutrinos are in general not identical to the mass eigenstates and the Pontecorvo-Maki-Nakgawa-Sakata (PMNS) mixing matrix needs to be added [7]. The resulting Dirac mass term is however not the only possibility to achieve massive neutrinos. An alternative is a Majorana mass term:

$$\mathcal{L}_{\mathrm{Majorana}} = -m_M \left(\bar{\psi}^c_{\nu,L}\psi_{\nu,L} + \mathrm{h.c.}\right) \tag{1.16}$$

However, this contribution does not conserve the lepton number and may give rise to a neutrino-less nuclear double beta decay, which is not observed, yet [8].

The symmetry breaking induces a mixing of the neutral boson field W^3 and B, which can be diagonalised by

$$Z_\mu = \cos\theta_{\mathrm{w}} W^3_\mu - \sin\theta_{\mathrm{w}} B_\mu \tag{1.17}$$

$$A_\mu = \sin\theta_{\mathrm{w}} W^3_\mu + \cos\theta_{\mathrm{w}} B_\mu\ , \tag{1.18}$$

where the physical photon and Z boson fields A_μ and Z_μ, appear. The weak mixing angle θ_{w} is define by the ratio of the coupling constants g_1 and g_2:

$$\tan\theta_{\mathrm{w}} = \frac{g_1}{g_2} \tag{1.19}$$

The gauge boson masses are found to be

$$M_\gamma = 0,\quad M_{\mathrm{W}} = \frac{v}{2} g_2,\quad M_{\mathrm{Z}} = \frac{v}{2}\sqrt{g_1^2 + g_2^2}\ . \tag{1.20}$$

The photon is indeed massless. An important result is the relation of the ratio of the heavy gauge boson masses to the weak mixing angle:

$$\frac{M_{\mathrm{W}}}{M_{\mathrm{Z}}} = \cos\theta_{\mathrm{w}}\ . \tag{1.21}$$

This mixing angle also appears in the boson-fermion couplings which becomes more evident when the interaction term is phrased in terms of currents:

$$\mathcal{L}_{\text{int}} = -e \left\{ A_\mu J^\mu_{\text{em}} + \frac{1}{\sqrt{2}\sin\theta_{\text{w}}} \left(W^+_\mu J^\mu_{\text{CC}} + W^-_\mu J^{\mu\dagger}_{\text{CC}} \right) + \frac{1}{\sin\theta_{\text{w}}\cos\theta_{\text{w}}} Z_\mu J^\mu_{\text{NC}} \right\} . \tag{1.22}$$

The J^μ denote the electromagnetic, charged and neutral current of each fermion fiel ψ_f

$$J^\mu_{\text{em}} = \bar{\psi}_f \gamma^\mu (T_3 + Y) \psi_f \tag{1.23}$$
$$J^\mu_{\text{CC}} = \bar{\psi}_f \gamma^\mu (T_1 + i T_2) \psi_f \tag{1.24}$$
$$J^\mu_{\text{NC}} = \bar{\psi}_f \gamma^\mu T_3 \psi_f - \sin^2\theta_{\text{w}} J^\mu_{\text{em}} . \tag{1.25}$$

In the firs term the electrical charge is identifie with $Q = T_3 + Y$. The charged current term describes W boson production and decay into chiral fermions:

$$J^\mu_{\text{CC}} = \frac{1}{2} \bar{\psi}_f \gamma^\mu (1 - \gamma_5) \psi_f . \tag{1.26}$$

The neutral current is usually written in a more general way to split vector and axial-vector currents:

$$J^\mu_{\text{NC}} = \frac{1}{2} \bar{\psi}_f \left(g^{\text{f}}_{\text{V}} \gamma^\mu - g^{\text{f}}_{\text{A}} \gamma^\mu \gamma_5 \right) \psi_f , \tag{1.27}$$

with the coupling constants

$$g^{\text{f}}_{\text{V}} = T_3 - 2Q \sin^2\theta_{\text{w}} \tag{1.28}$$
$$g^{\text{f}}_{\text{A}} = T_3 , \tag{1.29}$$

and with T_3 and Q according to Table 1.1. This relates the electromagnetic coupling e to the electroweak couplings g_1 and g_2

$$e = g_1 \cos\theta_{\text{w}} = g_2 \sin\theta_{\text{w}} \tag{1.30}$$

The classical Fermi interaction of charged currents

$$\mathcal{L}_{\text{Fermi}} = -\frac{G_{\text{F}}}{\sqrt{2}} J^\dagger_{\mu,\text{CC}} J^\mu_{\text{CC}} \tag{1.31}$$

is a second order process in the Standard Model mediated by W exchange. In the limit of small momentum transfer the Fermi constant G_{F} becomes

$$G_{\mathrm{F}} = \frac{g_2^2}{4\sqrt{2}M_{\mathrm{W}}^2} \,. \tag{1.32}$$

The constant G_{F} is determined in muon lifetime measurements to the current world-average value of $G_{\mathrm{F}} = 1.16637(1) \times 10^{-5}$ GeV^{-2} [3]. The W-mass can therefore be calculated at tree level:

$$M_{\mathrm{W}} = \frac{\pi \alpha_{\mathrm{QED}}}{\sin^2 \theta_{\mathrm{w}} \sqrt{2} G_{\mathrm{F}}} \tag{1.33}$$

with the electromagnetic $\alpha_{\mathrm{QED}} = e^2/4\pi$. This implies

$$v = \frac{1}{\sqrt{\sqrt{2}G_{\mathrm{F}}}} \,. \tag{1.34}$$

which numerically is equal to $v = 246.221(2)$ GeV. All mass terms in the Standard Model are proportional to v. Apart from the gauge bosons, no other particle mass is however fi ed by only this value but involves a second free parameter.

The physical manifestation of the Higgs mechanism, the neutral Higgs boson, H, interacts with the fermions and gauge bosons. The interaction Lagrangian is given by:

$$\mathcal{L}_{\mathrm{H,int}} = -\frac{m_{\mathrm{f}}}{v} H \bar{\psi}_f \psi_f + \frac{M_{\mathrm{W}}^2}{v^2} W_\mu^- W_+^\mu \left(H^2 + 2vH\right) + \frac{M_Z^2}{2v^2} Z_\mu Z^\mu \left(H^2 + 2vH\right) \tag{1.35}$$

and the lowest order Feynman diagrams are shown in Fig. 1.1. The Higgs couplings to fermions and vector bosons, Hff, HVV, and $HHVV$, depend directly on the particle masses:

$$g_{Hff} = i\frac{m_{\mathrm{f}}}{v} \;;\; g_{HVV} = -2i\frac{M_{\mathrm{V}}^2}{v} \;;\; g_{HHVV} = -2i\frac{M_{\mathrm{V}}^2}{v^2} \,. \tag{1.36}$$

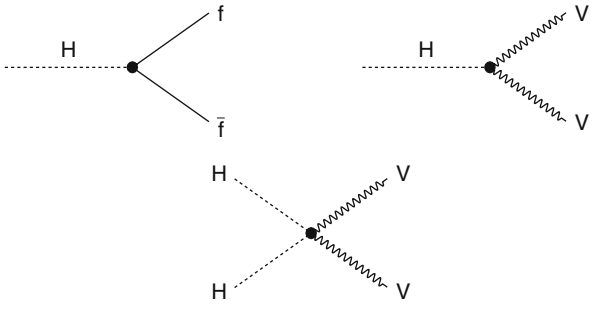

Fig. 1.1 Lowest order Feynman diagrams of Higgs boson couplings to fermions, f, and massive gauge bosons, V = W, Z

The Higgs boson has not been discovered experimentally, yet. The coupling structure is therefore important in the corresponding searches, since it is expected to couple to the heaviest particles that is kinematically allowed. Important production and decay channels with massless particles, like gluons and photons, are possible via loops, which is described later in more detail.

Indications about the energy scale of the mass of the Higgs boson can be derived from several arguments. The unitarity bound on longitudinal gauge boson scattering [9] requires new physics in the TeV energy scale. If it is the Higgs boson that dresses the scattering amplitude to not exceed the unitarity limit, the mass of the Higgs boson should not exceed 870 GeV (at tree level and in the high-energy limit [10]). Furthermore, the Higgs width into vector bosons increases to lowest order with M_{H}^3/v^2. The particle character of the Higgs boson requires that the width should not exceed M_{H}, which limits M_{H} to about 1.4 TeV [10].

Quantum effects of the Higgs self-interaction potential

$$\mathcal{L}_{\mathrm{H,self}} = \lambda v H^3 + \frac{\lambda}{4} H^4 \tag{1.37}$$

lead to additional theoretical constraints. The renormalisation group equation for the Higgs self-coupling λ behaves to firs order and in the limit of large momentum transfer, $Q^2 \gg 0$, according to [11]

$$\lambda(Q^2) = \lambda(v) \frac{1}{1 - \frac{3}{4\pi^2}\lambda(v^2) \log \frac{Q^2}{v^2}} \,. \tag{1.38}$$

This means that the coupling has a Landau pole at $\Lambda_C = v e^{\frac{4\pi^2 v^2}{3M_{\mathrm{H}}^2}}$, where it becomes infinite This typical behaviour of a ϕ^4 theory shows that it is only an effective theory up to the scale Λ_C. Thus, if Λ_C is set to the very high energies of the "grand unification (GUT) scale of about 10^{16} GeV, the Higgs mass must not exceed ≈ 250 GeV for the theory to remain valid. This triviality bound is shown graphically in Fig. 1.2. One must however keep in mind that in case of large values of λ, perturbation theory will break down. On the other hand, lattice calculations show that this limit still stays in the range of $M_{\mathrm{H}} < 710$ GeV [11].

A lower limit on M_{H} is derived from the stability of the Higgs potential [5]. Quantum corrections to $HH \to HH$ scattering with fermion and vector boson loops tend to push $\lambda(Q^2)$ to negative values. In the small coupling limit, one obtains:

$$\lambda(Q^2) = \lambda(v^2) + \frac{1}{16\pi^2} \left\{ -12 \frac{m_{\mathrm{t}}^4}{v^4} + \frac{3}{16} \left(2g_2^4 + \left(g_2^2 + g_1^2 \right)^2 \right) \right\} \log \frac{Q^2}{v^2} \tag{1.39}$$

which can become negative if $\lambda(v^2)$ is small. The Higgs potential then develops a new minimum $V(|Q|) < V(v)$, which is not stable. To avoid the instability, the Higgs mass should fulfi

$$M_H^2 = 2\lambda(v^2)v^2 > -\frac{v^2}{8\pi^2}\left\{-12\frac{m_t^4}{v^4} + \frac{3}{16}\left(2g_2^4 + \left(g_2^2 + g_1^2\right)^2\right)\right\}\log\frac{Q^2}{v^2}\ , \quad (1.40)$$

which depends mainly on the top quark mass, m_t, and the values of the gauge couplings, g_i. This yields $M_H > 370$ GeV for $\Lambda_C = 10^{16}$ GeV. A more accurate calculation [12, 13] results in $M_H > 125$ GeV, depicted as vacuum stability bound in Fig. 1.2.

However, the vacuum could also be meta-stable and the electroweak minimum may differ from the absolute minimum of the effective theory. To avoid significan tunnelling probability between the two vacua, the Higgs mass should also not exceed some minimal value, which is about 10–15 GeV lower than the normal stability bound [13].

The fermion and boson loop corrections to the Higgs propagator relate the physical Higgs mass, M_H, to the "bare" mass, M_H^0, of the unrenormalised Lagrangian. The corresponding lowest order diagrams are shown in Fig. 1.3. Cutting the loop integral momenta at a scale Λ one obtains in the limit of a large top quark mass at lowest order [5]:

$$M_H^2 = \left(M_H^0\right)^2 + \frac{3\Lambda^2}{8\pi^2 v^2}\left[M_H^2 + 2M_W^2 + M_Z^2 - 4m_t^2\right]\ . \quad (1.41)$$

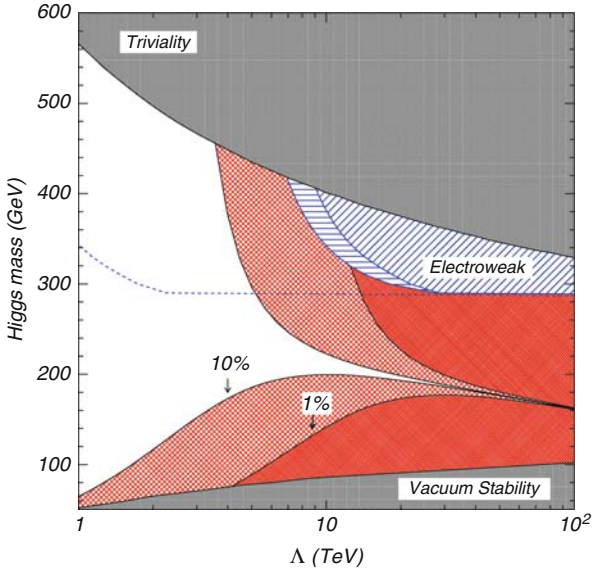

Fig. 1.2 The theoretical bounds [14] on M_H from vacuum stability (*lower bounds*) and triviality (*upper bound*) are shown as *grey areas*. They indicate the limiting values of M_H between which the Standard Model remains valid up to the energy scale Λ. The hatched regions indicate where fine tuning at the level of 1 and 10% is necessary. The *white region* corresponds to the parameter range where all constraints are fulfille without much fine-tunin (> 10%). The analysis of electroweak data leads to further constrains on M_H, indicated by the *dashed area*

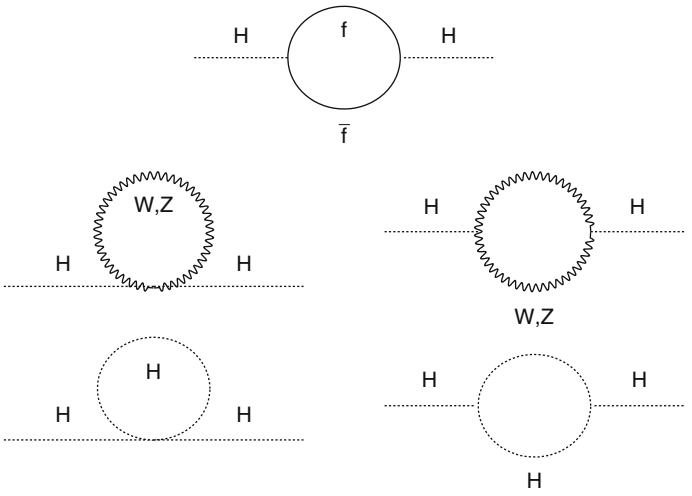

Fig. 1.3 Feynman diagrams of the one-loop corrections to the Standard Model Higgs boson mass

Now, if Λ is chosen to be at large energy scales of 10^{16} GeV, the parameter M_{H}^0 must be tuned properly to 16 digits to get M_{H} right. Another solution would be to avoid the quadratic divergence by choosing $M_{\mathrm{H}}^2 = -\left(2M_{\mathrm{W}}^2 + M_{\mathrm{Z}}^2 - 4m_{\mathrm{t}}^2\right)$ [15]. This is however not valid at higher orders, and the fine-tunin problem remains. Figure 1.2 shows how much fine-tunin is needed assuming the validity of the Standard Model up to a given scale Λ. Only for $M_{\mathrm{H}} \approx 200$ GeV, fine-tunin is in a reasonable range ($> 10\%$) also at high energies. This is the most stringent theoretical constraint within the Standard Model as a perturbative theory.

Eventually, also cosmological arguments which involve the formation of large scale structures of the universe due to the so-called inflatio model [16] can constrain the shape of the Higgs potential. Assuming that it is the Standard Model Higgs fiel that initiates inflatio and with certain conditions on the Higgs gravitational coupling [17], a limit of $M_{\mathrm{H}} \in [126, 194]$ GeV can be derived.

In summary, the rather general unitary bound requires new physics at the 1 TeV scale, which in the Standard Model should appear in form of the scalar Higgs boson. Further theoretical constraints indicate that $M_{\mathrm{H}} \approx 200$ GeV if the Standard Model shall remain valid to very high energy scales.

1.2 Quantum Chromodynamics

Strong interactions of quark field ψ_q and gluon field G_μ are described in the Standard Model Lagrangian by the following term:

$$\mathcal{L}_{\mathrm{colour}} = -\frac{1}{4} F_a^{\mu\nu} F_{\mu\nu}^a + \sum_q i\bar{\psi}_{q,j}\gamma^\mu \left(\partial_\mu - i g_3 G_\mu^a \frac{\lambda_a}{2}\right)\psi_{q,k} \,. \tag{1.42}$$

where $a = 1, \ldots, 8$ and $j, k = 1, 2, 3$ denote the colour indices for gluons and quarks, respectively. The sum extends over all quarks *u,d,s,c,t,b*. The gauge fiel strength of the gluon field G_μ is given by

$$F^a_{\mu\nu} = \partial_\mu G^a_\nu - \partial_\nu G^a_\mu - g_3 f^{abc} G^b_\mu G^c_\nu \,. \tag{1.43}$$

The constant g_3 is the coupling parameter and the factors f^{abc} are the $SU(3)$ structure constants. The λ^a matrices denote the three-dimensional representation of the group generators of the $SU(3)$.

Since quark-gluon and gluon-gluon interactions are proportional to g_3^2 one introduces the strong coupling constant $\alpha_s = g_3^2/4\pi$. The most interesting property of QCD is the behaviour of α_s: when virtual corrections due to the gluon fiel are taken into account, the strong coupling changes with momentum transfer q^2 like:

$$\alpha_s(q^2) = \frac{12\pi}{(33 - 2n_f)\log\left(q^2/\Lambda^2_{\mathrm{QCD}}\right)} \tag{1.44}$$

with the QCD energy scale Λ_{QCD} and the number of quark fl vours n_f with quark masses lower than $\sqrt{q^2}$. This means that the value of α_s decreases with increasing q^2. This effect is known as asymptotic freedom. However, the opposite behaviour is seen with decreasing q^2: the coupling strength increases. This has the consequence that no free coloured objects are observed in nature, and quarks and gluons are bound by the principle of colour confinement The running of α_s is nicely confirme in measurements which are compiled in [18].

The predictions of perturbative QCD are successfully applied when quarks and gluons can be considered as free particles, which is usually the case in the high energy regime where effects of colour confinemen can be neglected. The transition from coloured quarks and gluons to the colourless hadronic particles in the fina state of a physics reaction is however difficul to describe from firs principles. In theoretical calculations, Monte Carlo models are an effective approach to cover the fragmentation and hadronisation phase of the physics process. The most common models are described at the end of this chapter.

1.3 Electroweak Radiative Corrections

Higher-order radiative corrections need to be taken into account for the theoretical calculations to match the precision of the measurements. They also lead to more involved relations between the Standard Model parameters, which are

- the fermion masses, m_{f}
- the electroweak boson masses, M_{W}, M_{Z}
- the mass of the Higgs boson, M_{H}
- the electromagnetic and strong coupling constants, α_{QED} and α_s
- the elements of the CKM mixing matrix and, in an extension to the Standard Model, those of the neutrino mixing matrix.

The coupling constants that appear in the charged and neutral current interactions are in principle functions of these parameters and of the quantum numbers of the interacting particles. The non-trivial relations between coupling and mass measurements are tested in a combined analysis to accept or reject the theoretical model.

The tree-level Eq. (1.33), which relates the W boson mass to the Z boson mass, is modifie in the following way:

$$M_{\mathrm{W}}^2\left(1-\frac{M_{\mathrm{W}}^2}{M_{\mathrm{Z}}^2}\right)=\frac{\pi\alpha_{\mathrm{QED}}}{\sqrt{2}G_{\mathrm{F}}}\times\frac{1}{1-\Delta r} \tag{1.45}$$

The Δr term is due to propagator corrections caused by loop diagrams, as shown in Fig. 1.4. They can by split into QED corrections, $\Delta\alpha_{\mathrm{QED}}$, to the photon propagator, electroweak corrections, $\Delta\rho$, and an electroweak remainder term, $\Delta r_{\mathrm{remainder}}$:

$$\Delta r=\Delta\alpha_{\mathrm{QED}}-\frac{\cos^2\theta_{\mathrm{w}}}{\sin^2\theta_{\mathrm{w}}}\Delta\rho+\Delta r_{\mathrm{remainder}} \tag{1.46}$$

The QED corrections are related to the photon self-energy which change the electromagnetic coupling for non-zero momentum transfer q^2:

$$\alpha_{\mathrm{QED}}(q^2)=\alpha_{\mathrm{QED}}(0)\frac{1}{1-\Delta\alpha_{\mathrm{QED}}(q^2)} \tag{1.47}$$

where $\alpha_{\mathrm{QED}}(0)=1/137.035999679(94)$ [19]. The most interesting value is the correction at the Z-pole, $q^2=M_{\mathrm{Z}}^2$, because many precision measurements are carried out at this centre-of-mass energy.

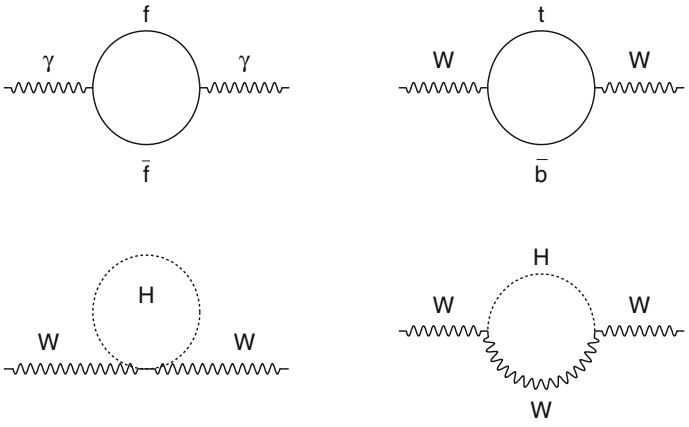

Fig. 1.4 Feynman diagrams showing leading order loop corrections to the vector boson propagators

Each fermion with mass $m < \sqrt{q^2}$ contributes to $\Delta\alpha(M_Z^2)$. The leptonic correction has been calculated to third order to be $\Delta\alpha_\ell = 0.03150$ [20] with negligible uncertainty. The corrections due to quark loops require a more detailed analysis because there are potentially large QCD corrections to be taken into account. The top quark term, $\Delta\alpha_{\text{top}}$, is treated separately since it depends on the top mass. Its value is $\Delta\alpha_{\text{top}} = -0.00007(1)$ [21]. The light quark term, $\Delta\alpha_{\text{had}}^{(5)}$, is usually calculated from measurements of the hadronic cross-section in e^+e^- collisions at centre-of-mass energies, $\sqrt{s}$, well below the Z pole, $\sqrt{s} \ll M_Z$. An experimentally driven evaluation yields $\Delta\alpha_{\text{had}}^{(5)} = 0.02758 \pm 0.0035$ [22]. This correction gives the largest uncertainty to $\Delta\alpha(M_Z^2)$.

The ρ parameter is define as

$$\rho = \frac{1}{\cos^2\theta_{\text{w}}} \times \frac{M_{\text{W}}^2}{M_{\text{Z}}^2} \tag{1.48}$$

and has a value of 1 at tree level. The quantum corrections to this relation is mainly determined by the self-energy of the W boson propagator. It is sensitive to all $SU(2)$ multiplets which directly couple to gauge bosons and exhibit a large mass splitting. The mass differences in the light quark multiplets are in general small. The leading term is therefore given by the $t - b$ loop:

$$\Delta\rho_t = 3\frac{G_{\text{F}} m_{\text{t}}^2}{8\pi^2\sqrt{2}} = 0.00939 \pm 0.00014 \tag{1.49}$$

in the approximation $m_{\text{t}} \gg m_b$, and using the recent measurement of the top quark mass, $m_{\text{t}} = 173.1 \pm 1.3$ GeV [23], by the CDF and DØ collaborations.

Higgs boson contributions to $\Delta\rho$ are playing an interesting role in the analysis of measurements in the framework of the Standard Model. The corrections are

$$\Delta\rho_H = -3\frac{G_{\text{F}} M_{\text{W}}^2}{8\pi^2\sqrt{2}} \tan^2\theta_{\text{w}} \left(\log\frac{M_{\text{H}}^2}{M_{\text{W}}^2} - \frac{5}{6}\right) \tag{1.50}$$

for $M_{\text{H}} \gg M_{\text{W}}$.

Also in the remainder term Higgs and top quark contributions appear:

$$\begin{aligned}\Delta r_{t,\text{rem}} = & -\frac{G_{\text{F}} M_{\text{W}}^2}{8\pi^2\sqrt{2}} \left\{ 3\cot^2\theta_{\text{w}} \frac{m_{\text{t}}^2}{M_{\text{W}}^2} + 2\left(\cot^2\theta_{\text{w}} - \frac{1}{3}\right)\log\frac{m_{\text{t}}^2}{M_{\text{W}}^2} \right. \\ & \left. + \frac{4}{3}\log\cos^2\theta_{\text{w}} + \cot^2\theta_{\text{w}} - \frac{7}{9} \right\} \end{aligned} \tag{1.51}$$

$$\Delta r_{H,\text{rem}} = \frac{\sqrt{2} G_{\text{F}} M_{\text{W}}^2}{16\pi^2} \left\{ \frac{11}{3}\left(\log\frac{M_{\text{H}}^2}{M_{\text{W}}^2} - \frac{5}{6}\right) \right\} , \tag{1.52}$$

again for $M_{\text{H}} \gg M_{\text{W}}$.

Radiative corrections are as well important in the determination of the Z couplings to the fermions, $g_{\mathrm{V}}^{\mathrm{f}}$ and $g_{\mathrm{A}}^{\mathrm{f}}$, and their effective values are define as

$$g_{\mathrm{V}}^{\mathrm{f,eff}} = \sqrt{\rho_{\mathrm{f}}}\left(T_3 - 2Q_{\mathrm{f}}\sin^2\theta_{\mathrm{eff}}^{\mathrm{f}}\right) \tag{1.53}$$

$$g_{\mathrm{A}}^{\mathrm{f,eff}} = \sqrt{\rho_{\mathrm{f}}}T_3 \tag{1.54}$$

with an effective weak mixing angle, $\sin^2\theta_{\mathrm{eff}}^{\mathrm{f}}$, and the ρ_{f} parameter which includes universal Z propagator and fl vour specifi vertex corrections. This eliminates the dependency of the measurements on radiative corrections and reduces the measurement uncertainty. Using this definition the ratio of the effective vector and axial-vector coupling is directly related to the effective weak mixing angle, given by

$$\sin^2\theta_{\mathrm{eff}} = \frac{1}{4}\left(1 - \frac{g_{\mathrm{V}}^{\mathrm{eff}}}{g_{\mathrm{A}}^{\mathrm{eff}}}\right) \tag{1.55}$$

There is an effective angle for each type of fermion, which is proportional to the on-shell definitio of the mixing angle (see Eq. (1.21)):

$$\sin^2\theta_{\mathrm{eff}}^{\mathrm{f}} = \kappa_{\mathrm{f}}\sin^2\theta_{\mathrm{w}}\,. \tag{1.56}$$

The factor κ_{f} is related to the radiative correction term Δr_{f} by the following equation:

$$\sqrt{2}G_{\mathrm{F}}M_{\mathrm{Z}}^2\sin^2\theta_{\mathrm{eff}}^{\mathrm{f}}\cos^2\theta_{\mathrm{eff}}^{\mathrm{f}} = \frac{\pi\alpha_{\mathrm{QED}}}{1-\Delta r_{\mathrm{f}}}\,. \tag{1.57}$$

The quantity Δr_{f} is very similar to the one that is given in Eq. (1.46):

$$\Delta r_{\mathrm{f}} = \Delta\alpha_{\mathrm{QED}} - \frac{\cos^2\theta_{\mathrm{w}}}{\sin^2\theta_{\mathrm{w}}}\Delta\rho + \Delta r_{\mathrm{f,rem}}\,. \tag{1.58}$$

Only the last term $\Delta r_{\mathrm{f,rem}}$ is define differently and takes additional $\mathrm{Z}/\gamma\to\mathrm{f}\bar{\mathrm{f}}$ vertex corrections into account. A more detailed discussion can be found in [24].

Current calculations include electroweak radiative corrections at two-loop order to the W boson propagator. Complete fermionic two-loop results are available for the determination of $\sin^2\theta_{\mathrm{eff}}^{\ell}$. In the limit of large m_{t} the top contributions to $\Delta\rho$ are known to three-loop order.

Since precision measurements are well sensitive to these small quantum corrections there is sensitivity to the mass of the Higgs boson, which is the only particle of the Standard Model that has not been observed, yet. Other indirect determinations of Standard Model parameters work out well. The derived mass of the W boson $M_{\mathrm{W}} = 80.364 \pm 0.020$ GeV agrees well with the direct measurement at LEP and Tevatron of $M_{\mathrm{W}} = 80.399 \pm 0.023$ GeV. The indirect top quark mass $m_{\mathrm{t}} = 179.3^{+11.6}_{-8.5}$ GeV [26] has a much lower precision than the direct measurement by CDF and DØ, $m_{\mathrm{t}} = 173.1 \pm 1.3$ GeV [23], but also here the agreement is very

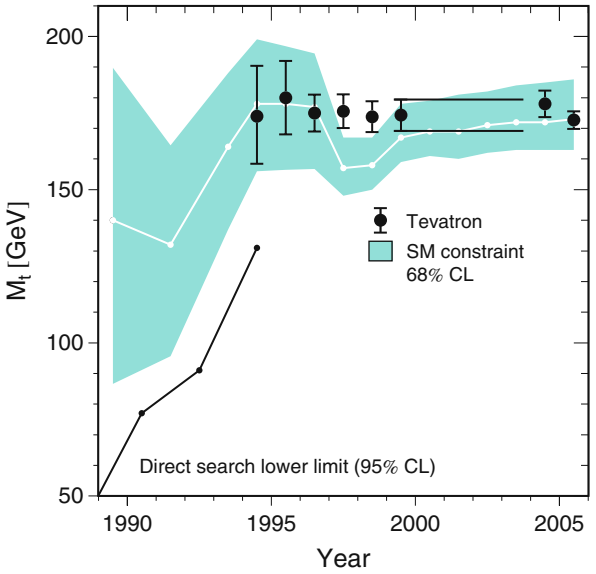

Fig. 1.5 Historic development of the indirect limits on the top mass, the direct search limits and eventually the measurements at the Tevatron [25]

good. In fact, the discovery of the top quark was lead by more and more precise model predictions. The historical development of these calculations and the firs measurements are compared in Fig. 1.5. This gives confidenc that also the indirect information on M_{H} is useful within the Standard Model framework.

From the analysis of electroweak precision measurements alone, an upper limit of 157 GeV at 95% confidenc level (C.L.) can be derived [26]. Combined with direct searches for the Higgs boson at LEP [27], this constraint is weakened slightly and a 95% C.L. range of $114.4\ \mathrm{GeV} < M_{\mathrm{H}} < 186\ \mathrm{GeV}$ for the mass of the Higgs boson is determined [26]. This is well in the reach of the LHC and Higgs boson searches and dedicated analyses concentrate on the low M_{H} region.

1.4 Extensions to the Standard Model

The most attractive theoretical extension to the Standard Model is super-symmetry (SUSY), which is introducing a global symmetry between bosons and fermions by changing the spin by $\pm 1/2$ units. The corresponding operators, Q_α, transform fermions into bosons and vice-versa:

$$Q|\mathrm{Fermion}\rangle = |\mathrm{Boson}\rangle\ ; \quad Q|\mathrm{Boson}\rangle = |\mathrm{Fermion}\rangle \tag{1.59}$$

They are spinors and follow the SUSY algebra:

$$\{Q_\alpha, \bar{Q}_\beta\} = -(g^\mu)_{\alpha\beta} P_\mu\ , \tag{1.60}$$

where P_μ is the momentum generator of space-time translations. The particle spectrum of the Standard Model is preserved and extended by super-symmetric partners of the known elementary particles. The partners of fermions are scalar sfermions, and the gauge boson sector is mapped to spin-1/2 gauginos. Super-symmetric models overcome some of the deficit of the Standard Model. If SUSY is exact, the fine tuning problem is resolved due to opposite-sign loop contributions from fermions and bosons. However, the symmetry can evidently not be exact and is broken at some SUSY energy scale, since the not yet discovered SUSY partners must be of larger mass than the currently known Standard Model particles.

In super-symmetric models the Higgs-sector is necessarily extended to two Higgs doublets to avoid anomalies and to provide super-symmetric mass terms for up- and down-type fermions. The firs doublet, H_1, is giving masses to the down-type fermions and the second, H_2, introduces masses to the up-type fermions. This results in three neutral Higgs bosons, h^0, H^0, A^0, and one charged Higgs boson, $H^\pm$. The neutral Higgs field h^0 and H^0 are CP even, while the A^0 fiel is CP odd. The super-partners of the weak gauge bosons and the Higgs super-partners actually mix and form neutralinos, $\tilde{\chi}^0_{1,2,3,4}$, and charginos, $\tilde{\chi}^\pm_{1,2}$.

An important parameter of SUSY is the ratio of the vacuum expectation values, $\tan\beta = v_2/v_1$, of the Higgs doublet fields Taking the splitting of the mass scale of up- and down-type fermions into account, one can argue that $\tan\beta$ should be in the order of $m_t/m_b \approx 40$. Experimental constraints will be discussed later (see Chap. 4).

SUSY particle production is usually studied within the gravity and gauge mediated minimal SUSY models Minimal Super-Gravity (mSUGRA)) [28] and Gauge-Mediated Super-symmetry Breaking (GMSB) [29]. Benchmark scenarios are chosen to cover a wide range of experimental signatures. In both models, R-parity define as $R = (-1)^{3B+L+2S}$ with lepton number, L, baryon number, B, and spin, S, is conserved. As a consequence, SUSY particles can only be produced in pairs and the lightest SUSY particle (LSP) is stable. This leads to typical detector signatures from the SUSY decay chains since the LSP is expected to be only weakly interacting.

Typical mSUGRA models analysed at the LHC are for example, $SU1$, ..., $SU8.1$ [30], with different values of the universal sfermion and gaugino masses at the GUT scale, m_0 and $m_{1/2}$, of $\tan\beta = v_2/v_1$, of the sign of the Higgsino mass parameter, μ, and of the universal trilinear coupling, A_0, at the GUT scale. The next-to-leading order (NLO) total summed SUSY cross-section at LHC centre-of-mass energies of 14 TeV varies between 6 pb ($SU6$) and 402 pb ($SU4$) [31] for these models.

The cross-sections for SUSY Higgs production at the LHC is in the order of 1,000 pb for large $\tan\beta = 30$ and small Higgs masses of 100 GeV [5], down to 0.1 pb for large Higgs masses of 1,000 GeV. An interesting fact of SUSY models is the upper mass limit on the lightest Higgs boson, h, which is in the order of 110–130 GeV [33], depending on the mixing in the super-symmetric top sector. Because the couplings to up-type fermions are enhanced for $\tan\beta > 1$, the largest branching fraction of the h boson are to b-quark and τ lepton pairs ($\approx 90\%$ and $\approx$

10%, respectively). These are also the main decay channels of heavy CP-even Higgs bosons for large $\tan\beta$. For smaller values of $\tan\beta$ and 125 GeV $< M_{\mathrm{H}} <$ 250 GeV, the decays of the H boson are similar to the Standard Model Higgs boson, while for higher masses also the decay channels to h boson and top quark pairs open up. The CP-odd Higgs boson decays predominantly to $\mathrm{b\bar{b}}$ and $\tau^+\tau^-$ and for high masses to top quark pairs. The charged Higgs decays mainly to $\tau\nu$ for masses up to $M_{\mathrm{H}^\pm} \approx m_{\mathrm{t}}$, above which the tb fina state is preferred. These fina states are therefore the main search channels for super-symmetric Higgs bosons. The mass spectrum of the Higgs bosons depends mainly on the mass of the CP-odd Higgs boson, M_A, which is shown in Fig. 1.6, together with the different Higgs bosons that can be discovered at the LHC in different regions of the SUSY parameter space [32, 30].

In this work, however, only general aspects of SUSY will be discussed in the framework of the precision electroweak measurements. Further details can be found in [5, 30, 34, 35].

The Higgs sector may be enriched by adding more or higher Higgs multiplets. Such models are all constrained by the fact that the ρ parameter should not deviate too much from the measured value of 1. For a set of Higgs bosons with vacuum expectation values v_i, isospin I_i and third component I_i^3, the tree-level value of ρ is given by:

$$\rho = \frac{\sum_i \left\{ I_i(I_i+1) - \left(I_i^3\right)^2 \right\} v_i^2}{2\sum_i \left(I_i^3\right)^2 v_i^2} \,. \tag{1.61}$$

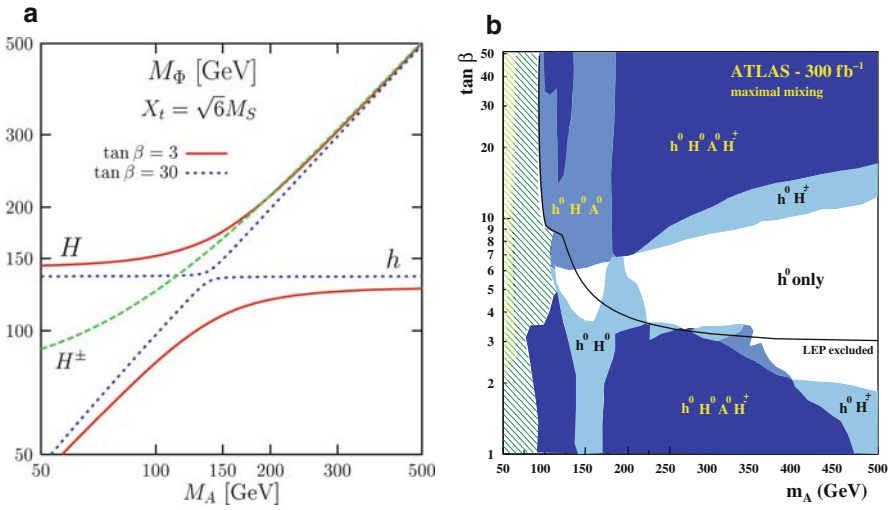

Fig. 1.6 (**a**) Super-symmetric Higgs boson masses as a function of the mass parameter, M_A, for the maximal top/stop mixing scenario [10]. (**b**) The number of SUSY Higgs bosons which can be discovered by the ATLAS experiment for different regions of the $M_A - \tan\beta$ plane assuming an integrated luminosity of 300 fb^{-1} [32]

For the Standard Model and multi-Higgs-doublet models, like SUSY, one always obtains a value of 1. If up- and down-type fermions would be of equal mass in each generation, $\rho = 1$ would hold exactly even at higher orders in the Standard Model since a larger $SU(2)_L \times SU(2)_R$ symmetry would be apparent. The top/bottom mass splitting is however breaking this symmetry. Higgs triplet models are possible extensions of the Standard Model and provide a mechanism for $SU(2)_L \times SU(2)_R$ symmetry breaking [36]. These models are also attractive because it is possible to construct neutrino mass terms compatible with current observations. One way to explain the smallness of the neutrino masses is the so-called see-saw mechanism which mixes right- and left-handed neutrinos such that heavy and light mass eigenstates evolve [37]. Mass terms of this kind can for example be constructed in Higgs triplet models. Experimentally, one should observe in addition to a rather light neutral Higgs boson [38], single- and double-charged Higgs boson, which are however not found, yet [39].

Higgs triplets are also predicted in Little Higgs models [40] in which the Higgs sector is dynamically generated by the interaction of originally massless scalar fields The Higgs is therefore a composite particle. However, new massive vector bosons and fermions as well as additional heavy up-type quarks are predicted in the model, which have not yet been seen in experiments.

Although the Higgs mechanism is very attractive for breaking electroweak symmetry and providing particle masses, there may be alternatives [41] which explain these phenomena without a Higgs field The strong $W_L W_L$ scattering must then be unitarized by some other states, e.g., techni-ρ particles in Technicolour models [42] or Kaluza-Klein (KK) gauge bosons in Higgs-less Models [43]. A generalised treatment of these models can be performed in terms of an effective Lagrangian method [44], which allows the study of possible effects in electroweak boson scattering and signatures at the LHC. New resonance states as well as anomalous scattering cross-sections can be expected in these scenarios.

A requirement of all more or less exotic extensions of the Standard Model is the necessity to be compatible with todays precise measurements in the electroweak sector. In the remaining part of this chapter the phenomenology of the most important Standard Model processes will therefore be discussed.

1.5 Z Boson Production and Decay in e^+e^- Collisions

The properties of the Z boson were studied in detail at LEP and SLD at energies around the Z pole. The following paragraphs summarise the most important observables that enter into the global analysis of electroweak data. Further details can be found in [45].

At energies below the W-pair threshold, Z bosons only decay to fermion pairs. The diagrams that contribute to the process $e^+e^- \to f\bar{f}$ at lowest order are shown in Fig. 1.7. The differential cross-section with photon and Z exchange, as well as their interference, can be written in the following way

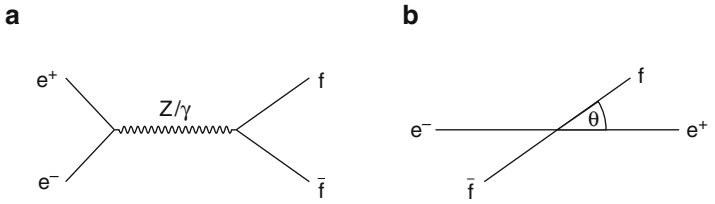

Fig. 1.7 (**a**) Feynman diagrams for fermion-pair production in e^+e^- collisions with photon and Z-boson exchange. (**b**) The scattering angle, θ, between incoming electron and fina state fermion

$$\begin{aligned}\frac{d\sigma}{d\cos\theta}(e^+e^- \to \bar{f}f) = \frac{\pi N_c^f}{2s}\Big\{&|\alpha(s)Q_f|^2(1+\cos^2\theta)\\ &-8Re\left(\alpha^* Q_f \chi(s)\left[\mathcal{G}_{Ve}\mathcal{G}_{Vf}(1+\cos^2\theta)+2\mathcal{G}_{Ae}\mathcal{G}_{Af}\cos\theta\right]\right)\\ &+16|\chi(s)|^2\left[(|\mathcal{G}_{Ve}|^2+|\mathcal{G}_{Ae}|^2)(|\mathcal{G}_{Vf}|^2+|\mathcal{G}_{Af}|^2)(1+\cos^2\theta)\right.\\ &\left.+8Re\left(\mathcal{G}_{Ve}\mathcal{G}_{Ae}^*\right)Re\left(\mathcal{G}_{Vf}\mathcal{G}_{Af}^*\right)\cos\theta\right]\Big\}\end{aligned} \tag{1.62}$$

where complex coupling constants $\alpha(s)$, $\mathcal{G}_{Vf}$, $\mathcal{G}_{Af}$ are used to absorb electroweak corrections (see [45]). Their real parts are related to the real couplings g_V^f and g_A^f by

$$\frac{g_V^f}{g_A^f} = Re\frac{\mathcal{G}_{Vf}}{\mathcal{G}_{Af}} = 1 - 4Q_f \sin^2\theta_{eff}^f\,. \tag{1.63}$$

The polar angle θ is the angle between the produced fermion and the incoming electron beam, as illustrated in Fig. 1.7. The propagator term

$$\chi(s) = \frac{G_F M_Z^2}{8\pi\sqrt{2}}\frac{s}{s - M_Z^2 + is\Gamma_Z/M_Z} \tag{1.64}$$

is define with an s-dependent width, $\Gamma_Z = \Gamma_Z(s)$. This is the convention used for all mass measurements at LEP. The alternative mass definitio as the real part of the complex pole corresponds to a propagator with an s-independent width:

$$\bar{\chi}(s) = \frac{G_F \bar{M}_Z^2}{8\pi\sqrt{2}}\frac{s}{s - \bar{M}_Z^2 + i\bar{\Gamma}_Z\bar{M}_Z}\,. \tag{1.65}$$

The two sets of variables are related by

$$M_Z = \bar{M}_Z\sqrt{1+\bar{\Gamma}_Z^2/\bar{M}_Z^2} \approx \bar{M}_Z + 34.1\ \text{MeV} \tag{1.66}$$

$$\bar{\Gamma}_Z = \bar{\Gamma}_Z\sqrt{1+\bar{\Gamma}_Z^2/\bar{M}_Z^2} \approx \bar{\Gamma}_Z + 0.9\ \text{MeV} \tag{1.67}$$

Both propagators lead to the same resonance shape $\sigma(s)$. For numerical results the s-dependent width scheme is used.

The partial width of the Z decaying into fermion pairs is given by

$$\Gamma_{f\bar{f}} = N_c^f \frac{G_F M_Z^3}{6\sqrt{2}\pi} \left(|\mathcal{G}_{Af}|^2 R_{Af} + |\mathcal{G}_{Vf}|^2 R_{Vf} \right) + \Delta_{ew,QCD} \tag{1.68}$$

The radiator factors R_{Vf} and R_{Af} take into account fina state QED and QCD corrections, while by $\Delta_{ew,QCD}$ small contributions from non-factorisable corrections are included. To firs order the R factors for axial and vector coupling are equal and given by

$$R_{Vf} = R_{Af} = R_f = R_{QED} R_{QCD} \tag{1.69}$$

with QED correction terms for all charged fermions

$$R_{QED} = 1 + \frac{3}{4} Q_f^2 \frac{\alpha(M_Z^2)}{\pi} + \dots \tag{1.70}$$

and QCD correction for quarks

$$R_{QCD} = 1 + \frac{\alpha_s(M_Z^2)}{\pi} + \dots \, . \tag{1.71}$$

This inclusive definitio of the fermionic decay width with quantum corrections simplifie the relation to the total decay width of the Z boson:

$$\Gamma_Z = \Gamma_{ee} + \Gamma_{\mu\mu} + \Gamma_{\tau\tau} + \Gamma_{had} + \Gamma_{inv} \tag{1.72}$$

where the hadronic width is the sum of the quark decay widths

$$\Gamma_{had} = \sum_{q \neq t} \Gamma_{q\bar{q}} \, . \tag{1.73}$$

The so-called invisible width sums up the contributions from neutrino decays

$$\Gamma_{inv} = N_\nu \Gamma_{\nu\bar{\nu}} \, . \tag{1.74}$$

The factor N_ν is the number of light neutrino generations and equal to 3 in the Standard Model. By measuring total and partial width of the Z boson this identity can be verifie experimentally.

Furthermore, the total cross-section of the $\cos\theta$-symmetric Z production term is written as

$$\sigma_{f\bar{f}}^Z = \frac{\sigma_{f\bar{f}}^0}{R_{QED}} \frac{s\Gamma_Z^2}{\left(s - M_Z^2\right)^2 + s^2\Gamma_Z^2/M_Z^2} \tag{1.75}$$

with the pole cross-section

$$\sigma^0_{\mathrm{f\bar{f}}} = \frac{12\pi}{M_Z^2}\frac{\Gamma_{\mathrm{ee}}\Gamma_{\mathrm{f\bar{f}}}}{\Gamma_Z^2} \,. \tag{1.76}$$

The hadronic pole cross-section σ^0_{had} and the hadronic to leptonic branching ratios

$$R^0_\ell = \frac{\Gamma_{\mathrm{had}}}{\Gamma_{\ell\ell}} \tag{1.77}$$

are observables that are included in the global analysis of electroweak data.

Since the axial couplings between Z and fermion, $g^{\mathrm{f}}_{\mathrm{A}}$, are non-zero, there is an asymmetry in the number of events with the fermion produced in the forward ($\theta > \pi/2$) and backward ($\theta < \pi/2$) hemispheres. This asymmetry is experimentally determined as

$$A_{\mathrm{FB}} = \frac{N_F - N_B}{N_F + N_B} \,, \tag{1.78}$$

where N_F is the number of events with a forward scattered fermion, and N_B the number of events with a backward scattered fermion. If only Z boson exchange is assumed the differential cross-section is simplified For the case of incoming polarised electrons and unpolarised positrons, and averaged over fina state helicities it is given by:

$$\frac{d\sigma_{\mathrm{f\bar{f}}}}{d\cos\theta} = \frac{3}{8}\sigma^{\mathrm{tot}}_{\mathrm{f\bar{f}}}\left[(1-\mathcal{P}_{\mathrm{e}}\mathcal{A}_{\mathrm{e}})(1+\cos^2\theta) + 2(\mathcal{A}_{\mathrm{e}} - \mathcal{P}_{\mathrm{e}})\mathcal{A}_{\mathrm{f}}\cos\theta\right] \,, \tag{1.79}$$

with the electron polarisation $\mathcal{P}_{\mathrm{e}}$ and the asymmetry parameter

$$\mathcal{A}_{\mathrm{f}} = \frac{2g^{\mathrm{f}}_{\mathrm{V}}g^{\mathrm{f}}_{\mathrm{A}}}{\left(g^{\mathrm{f}}_{\mathrm{V}}\right)^2 + \left(g^{\mathrm{f}}_{\mathrm{A}}\right)^2} \tag{1.80}$$

The forward-backward asymmetry is therefore equal to

$$A_{\mathrm{FB}} = \frac{\int_0^{+1}\frac{d\sigma_{\mathrm{f\bar{f}}}}{d\cos\theta}d\cos\theta - \int_{-1}^{0}\frac{d\sigma_{\mathrm{f\bar{f}}}}{d\cos\theta}d\cos\theta}{\int_{-1}^{+1}\frac{d\sigma_{\mathrm{f\bar{f}}}}{d\cos\theta}d\cos\theta} = \frac{\sigma_F - \sigma_B}{\sigma_F + \sigma_B} = \frac{3}{4}\mathcal{A}_{\mathrm{e}}\mathcal{A}_{\mathrm{f}} \,. \tag{1.81}$$

When the beam is polarised, the left-right asymmetry can be determined by measuring the event rate difference for positive and negative polarisation $\mathcal{P}_{\mathrm{e}}$ of the incoming electrons:

$$A_{\mathrm{LR}} = \frac{\sigma_L - \sigma_R}{\sigma_L + \sigma_R} = \mathcal{A}_{\mathrm{e}} \,. \tag{1.82}$$

And finall , the left-right forward-backward asymmetry is proportional to $\mathcal{A}_\mathrm{f}$:

$$A_{\mathrm{LR,FB}} = \frac{(\sigma_F - \sigma_B)_L - (\sigma_F - \sigma_B)_R}{(\sigma_F + \sigma_B)_L + (\sigma_F + \sigma_B)_R} \frac{1}{\langle |\mathcal{P}_\mathrm{e}| \rangle} = \frac{3}{4}\mathcal{A}_\mathrm{f} \tag{1.83}$$

In case of the tau lepton, also the fina state helicity can be measured. The correspond polarisation is define as

$$\mathcal{P}_\mathrm{f}(\cos\theta) = \frac{d(\sigma_r - \sigma_l)}{d\cos\theta} \left(\frac{d(\sigma_r + \sigma_l)}{d\cos\theta} \right)^{-1} \tag{1.84}$$

and given by

$$\mathcal{P}_\mathrm{f}(\cos\theta) = -\frac{\mathcal{A}_\mathrm{f}(1 + \cos^2\theta) + 2\mathcal{A}_\mathrm{e}\cos\theta}{(1 + \cos^2\theta) + 2\mathcal{A}_\mathrm{e}\mathcal{A}_\mathrm{f}\cos\theta} \tag{1.85}$$

and its average is

$$\langle \mathcal{P}_\mathrm{f} \rangle = -\mathcal{A}_\mathrm{f} \tag{1.86}$$

The asymmetry observables on the Z pole are define without further radiative corrections, unlike the Z decay widths. To extract the asymmetry from data the measurements are corrected for radiative effects, γ exchange and $\gamma - \mathrm{Z}$ interference terms. The pole quantities derived in this way are eventually

$$A_\mathrm{FB}^{0,\mathrm{f}} = \frac{3}{4}\mathcal{A}_\mathrm{e}\mathcal{A}_\mathrm{f} \tag{1.87}$$

$$A_\mathrm{LR}^{0} = \mathcal{A}_\mathrm{e} \tag{1.88}$$

$$A_{\mathrm{LR,FB}}^{0} = \frac{3}{4}\mathcal{A}_\mathrm{f} \tag{1.89}$$

$$\left\langle \mathcal{P}_\tau^0 \right\rangle = -\mathcal{A}_\tau \tag{1.90}$$

$$A_\mathrm{FB}^{\mathrm{pol},0} = -\frac{3}{4}\mathcal{A}_\mathrm{e} \tag{1.91}$$

Since the parameter $\mathcal{A}_\mathrm{e}$ is measured in left-right asymmetries independently from the forward-backward asymmetries, also the individual parameter $\mathcal{A}_\mu$, $\mathcal{A}_\tau$, $\mathcal{A}_\mathrm{b}$ and $\mathcal{A}_\mathrm{c}$ can be extracted. When expressing them as functions of the weak mixing angle one find from Eqs. (1.80) and (1.55):

$$\begin{aligned} \mathcal{A}_\mathrm{f} &= 2\frac{g_\mathrm{V}^\mathrm{f}/g_\mathrm{A}^\mathrm{f}}{1 + \left(g_\mathrm{V}^\mathrm{f}/g_\mathrm{A}^\mathrm{f}\right)^2} = 2\left(1 - 4|Q_\mathrm{f}|\sin^2\theta_\mathrm{eff}^\mathrm{f}\right) \frac{1}{\left(1 + \left(1 - 4|Q_\mathrm{f}|\sin^2\theta_\mathrm{eff}^\mathrm{f}\right)^2\right)} \\ &= \frac{1 - 4|Q_\mathrm{f}|\sin^2\theta_\mathrm{eff}^\mathrm{f}}{1 - 4|Q_\mathrm{f}|\sin^2\theta_\mathrm{eff}^\mathrm{f} + 8|Q_\mathrm{f}|^2\sin^4\theta_\mathrm{eff}^\mathrm{f}} \,. \end{aligned} \tag{1.92}$$

This shows that the determination of the asymmetry parameters is a sensitive measurement of $\sin^2\theta^{\mathrm{f}}_{\mathrm{eff}}$, deeply connected to the symmetry breaking mechanism of the Standard Model.

1.6 W Boson Production at LEP

The production of W boson pairs in e^+e^- collisions gives further handles for Standard Model tests. The W mass can be measured directly from the invariant mass of its decay products. Triple gauge boson couplings (TGC) of photon and Z to the W bosons as well as quartic couplings (QGC) can be determined from the analysis of the production angles and the polarisation of the W's. The fraction of longitudinal to transverse polarisation of the W bosons is measured as well.

To lowest order, the production of W-pairs is described by two Feynman diagrams, the t-channel neutrino exchange and the s-channel Z/γ exchange, as shown in Fig. 1.8. The diagram with a Higgs propagator is suppressed by a factor m_e/M_W and can be neglected. The s-channel graph involves the non-abelian gauge boson couplings, which are described later in more detail.

The lowest-order cross-section for on-shell production of W-pairs near the threshold is given by

$$\frac{d\sigma}{d\Omega} \approx \frac{\alpha^2_{\mathrm{QED}}}{s}\frac{1}{4\sin^4\theta_{\mathrm{w}}}\beta\left[1+4\beta\cos\theta\frac{3\cos^2\theta_{\mathrm{w}}-1}{4\cos^2\theta_{\mathrm{w}}-1}+O(\beta^2)\right]. \tag{1.93}$$

The leading term is proportional to the W velocity, β, and is from t-channel neutrino exchange. It is the dominating term in the production threshold region, where $\sqrt{s} \approx 2M_{\mathrm{W}}$. For the total cross section one find

$$\sigma \approx \frac{\pi\alpha^2_{\mathrm{QED}}}{s}\frac{1}{4\sin^4\theta_{\mathrm{w}}}4\beta + O(\beta^3) \tag{1.94}$$

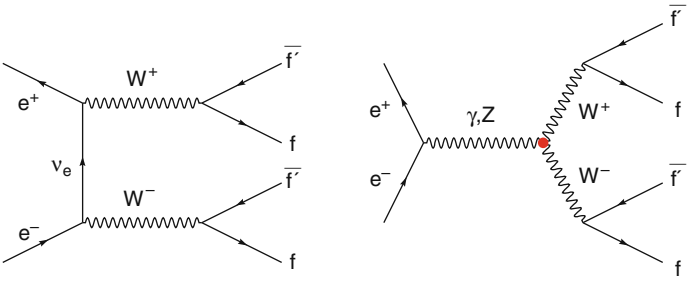

Fig. 1.8 Feynman diagrams for W-pair production at LEP with neutrino t-channel and Z/γ exchange

The terms proportional to β^2 drop out, and s-channel and interference contributions are only proportional to β^3. There is therefore no sensitivity to TGCs in the W-pair cross-section close to the threshold.

For a more complete description of the $e^+e^- \to WW$ process, also the decay of the W bosons needs to be taken into account. W bosons decay into pairs of quarks, one up-type and one down-type quark, $q\overline{q'}$, or a lepton and the corresponding neutrino, $\ell\nu_\ell$. Possible fina states are therefore fully hadronic qqqq, semi-leptonic $qq\ell\nu$, or fully leptonic $\ell\nu\ell\nu$. This makes W pair production part of the so-called four-fermion processes, $e^+e^- \to ffff$. They are usually denoted as charged current, CC, and neutral current, NC, processes, depending on the boson that is exchanged in the signal process. The number of diagrams that are contributing to each fina state in W-pair production is listed in Table 1.2. In this nomenclature, tree-level W-pair production is a CC03 process, while the complete description for the $qqe\nu$ fina state, e.g., is of type CC20.

The CC03 cross-section takes also off-shell W-pairs into account. In a simplifie form, the double-differential cross-section $\sigma_0^{\mathrm{CC03}}(s; s+, s-) = \frac{d\sigma^{\mathrm{CC03}}}{ds_+ ds_-}$ is folded with the Breit-Wigner propagator terms $\rho_W(s_\pm)$ [46]:

$$\sigma^{\mathrm{CC03}}(s) = \int_0^s ds_+ \int_0^{(\sqrt{s}-\sqrt{s_+})^2} ds_- \rho_W(s_+)\rho_W(s_-)\sigma_0^{\mathrm{CC03}}(s; s+, s-) \,, \tag{1.95}$$

where $s_+ = k_+^2$ and $s_- = k_-^2$ are the squared four-vectors of the internal W bosons. The Breit-Wigner factors are given by:

$$\rho_W(s_\pm) = \frac{1}{\pi} \frac{M_\mathrm{W}\Gamma_\mathrm{W}}{\left|s_\pm - M_\mathrm{W}^2 + iM_\mathrm{W}\Gamma_\mathrm{W}\right|^2} \times \mathrm{BR} \,, \tag{1.96}$$

with the branching fraction BR of the corresponding decay channel. The on-shell expression is recovered by letting the W width, Γ_W, go to zero:

$$\rho_W(s_\pm) \to \delta\left(s_\pm - M_\mathrm{W}^2\right) \times \mathrm{BR} \quad \text{for} \quad \Gamma_\mathrm{W} \to 0 \tag{1.97}$$

In the simple analytic approach the main corrections from initial state photon radiation (ISR) may be included as well. Photons emitted by the incoming electrons reduce the effective centre-of-mass energy, $\sqrt{s'} < \sqrt{s}$. In the case of a single photon

Table 1.2 Number of four-fermion diagrams for the different fina states in W-pair production

	$\bar{d}u$	$\bar{s}c$	$e^+\nu_e$	$\mu^+\nu_\mu$	$\tau^+\nu_\tau$
$d\bar{u}$	43	11	20	10	10
$s\bar{c}$	11	43	20	10	10
$e^-\bar{\nu}_e$	20	20	56	18	18
$\mu^-\bar{\nu}_\mu$	10	10	18	19	9
$\tau^-\bar{\nu}_\tau$	10	10	18	9	19

of energy E_γ radiated parallel to the beam, $\sqrt{s'}$ is given by

$$\sqrt{s'} = \sqrt{s}\sqrt{1 - \frac{2E_\gamma}{\sqrt{s}}} \,. \tag{1.98}$$

Photon emission with energy fractions x_i from each beam can be described by structure functions $D(x_i, s)$ which need to be convoluted

$$F(x, s) = \int_0^1 dx_1 dx_2 \delta(x - x_1 x_2) D(x_1, s) D(x_2, s) \tag{1.99}$$

The improved cross-section including ISR is then

$$\sigma^{\mathrm{CC03,ISR}}(s) = \int_{(s'/s)_{\min}}^{(s'/s)_{\max}} dx F(x, s) \int_0^{xs} ds_+ \int_0^{(\sqrt{xs}-\sqrt{s_+})^2} ds_- \rho_W(s_+)\rho_W(s_-)\sigma_0^{\mathrm{CC03}}(s; s+, s-) \,. \tag{1.100}$$

Figure 1.9 compares the lowest order calculations using GENTLE [47]. One observes that both the finit width and ISR effects lead to a broadening of the production threshold.

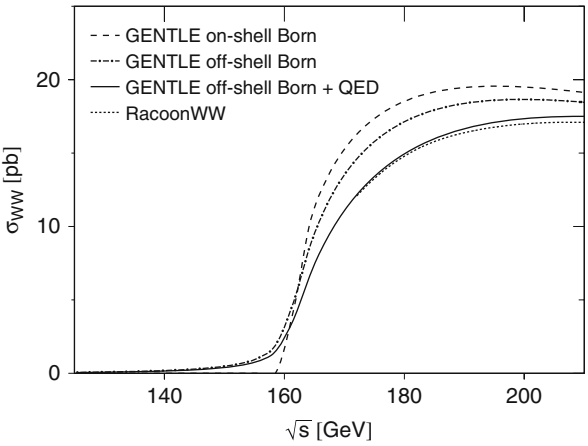

Fig. 1.9 Cross-section of W-pair production in e^+e^- collisions at lowest order, including W width effects, with ISR corrections calculated with GENTLE and the full $O(\alpha)$ calculation with RacoonWW

To eventually match the precision of the LEP measurements more complete radiative corrections need to be taken into account. The most recent predictions available in the RacoonWW [48] and KandY [49] Monte Carlo programs contain electroweak corrections at $O(\alpha)$. This brings the theoretical uncertainties on the cross-section to the level of 0.5% at centre-of-mass energies above 180 GeV. Around the threshold, $\sqrt{s} \approx 2M_{\mathrm{W}}$, the precision is only in the order of 2%. The improvement in accuracy in the higher energy range is due to the so-called leading or double-pole approximations (LPA/DPA) [50] which are applied to treat the virtual radiative corrections. In these approximations the matrix element is expanded around the resonant poles in powers of $\Gamma_{\mathrm{W}}/(M_{\mathrm{W}}\beta)$. The expansion is therefore only valid when the velocity β is sufficientl large, i.e. well above the W-pair threshold.

Recent results with better accuracy for the threshold region are obtained in an effective fiel theoretical approach [51]. In the analysis of LEP data they are not yet applied. But they may become important when a future e^+e^- linear collider will be operated at the W-pair threshold and large statistics data samples are collected.

1.7 Z and W Boson Production at Tevatron and the LHC

At $p\bar{p}$ and pp colliders the electroweak gauge bosons are produced as a single particle or in pairs through a parton-parton process, for example the Drell-Yann production of W and Z bosons, $q\bar{q} \to Z$ and $q\bar{q'} \to W$. The total cross-section of a certain process $pp \to X$ at a centre of mass energy $\sqrt{s}$ can be written as:

$$\sigma = \sum_{i,j} \int \hat{\sigma}_{ij}(\hat{s}, \mu_f, \mu_r) \int_0^1 \int_0^1 f_i\left(x_1, \mu_f^2\right) f_j\left(x_2, \mu_f^2\right) \delta(\hat{s} - x_1 x_2 s)\, dx_1\, dx_2\, d\hat{s}\ . \tag{1.101}$$

The different quantities in the equation are

$$\begin{aligned}
\hat{\sigma}_{ij} &= \text{parton-parton cross-section } i + j \to X \\
\sqrt{\hat{s}} &= \text{reduced centre-of-mass energy of the parton reaction } i + j \to X \\
x_1 &= \text{energy fraction of parton } i;\ x_1 = \frac{2E_1}{\sqrt{s}} \\
x_2 &= \text{energy fraction of parton } j;\ x_2 = \frac{2E_2}{\sqrt{s}} \\
f_i(x) &= \text{parton distribution function (PDF) for parton } i \text{ (same for } j\text{)} \\
&= \text{probability to fin parton } i \text{ with energy fraction } x \text{ inside the proton} \\
\mu_f &= \text{factorisation scale} \\
\mu_r &= \text{renormalisation scale}
\end{aligned}$$

The partons i and j may be quarks $(u, d, s, c, b, t, \bar{u}, \bar{d}, \bar{s}, \bar{c}, \bar{b}, \bar{t})$ and gluons inside the two protons of the colliding beams. The delta function $\delta(\hat{s} - x_1 x_2 s)$ ensures

the energy conservation. In the very simplifie case of the production of a narrow resonance the parton cross-section can be written as

$$\hat{\sigma}_{ij}(\hat{s}) = \sigma_{ij}\delta(\hat{s} - M^2)M^2 \tag{1.102}$$

where M is the mass of the resonance and σ_{ij} the (constant) cross-section of the reaction $i + j \to X$ at the peak of the resonance. The total cross-section is now simplifie to

$$\sigma = \sum_{i,j} \sigma_{ij} M^2 \times L_{ij} \tag{1.103}$$

with the parton-parton luminosity

$$L_{ij} = \frac{1}{s} \int_{\frac{M^2}{s}}^{1} \frac{1}{x} f_i(x) f_j \left(\frac{M^2}{xs} \right) dx \tag{1.104}$$

neglecting dependencies on factorisation and renormalisation scales in this notation. The rapidity of the resonance X is define as

$$y = \frac{1}{2} \log \frac{E - p_L}{E + p_L} \tag{1.105}$$

with energy E and longitudinal momentum p_L. It is well approximated by the more commonly used pseudo-rapidity

$$\eta = \frac{1}{2} \log \frac{|\mathbf{p}| - p_L}{|\mathbf{p}| + p_L} = -\log \tan \frac{\theta}{2} , \tag{1.106}$$

which can be directly measured in terms of the polar angle θ. The energy fraction, x, of the partons that produce the massive decay product at rapidity, y, is given by

$$x = \frac{M}{\sqrt{s}} e^{\pm y} \tag{1.107}$$

The differential rapidity distribution of X is therefore to lowest order proportional to the product of the parton density functions:

$$\frac{d\sigma}{dy}(pp \to X) = \sum_{i,j} \sigma_{ij} \frac{M^2}{s} f_i \left(\frac{M}{\sqrt{s}} e^{y} \right) f_j \left(\frac{M}{\sqrt{s}} e^{-y} \right) \tag{1.108}$$

Figure 1.10 shows the result of a proper calculation for W^+ and W^- production at the LHC simulated with a leading-order Monte Carlo program. One can observe a significan difference between the two charged bosons due to different quark contributions to the PDFs. This difference is planned be used in the determination of the parton luminosity at the LHC [52].

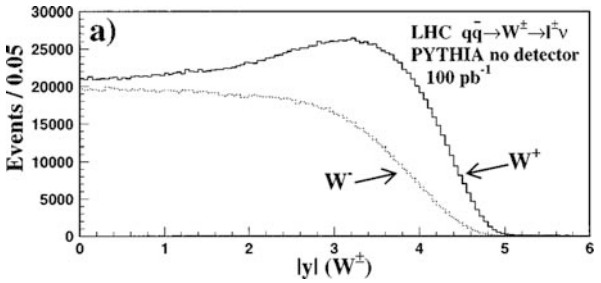

Fig. 1.10 Rapidity distribution at Monte Carlo generator level for W^+ and W^- production at LHC energies, taken from [52]

The simplifie picture must be extended by taking W and Z width effects into account, as well as QCD and QED radiative corrections. Taking higher order corrections at next-to-leading order (NLO) and beyond into account, typically reduces the scale dependencies on μ_r and μ_f of the cross-section predictions (see e.g. Sect. 6.1 and 6.3). The production of W and Z bosons accompanied by jets with large transverse momentum is also an important source of background for searches for new particles at hadron-hadron colliders.

Production cross-sections for various Standard Model processes are shown in Fig. 1.11, including some examples for vector bosons with exclusive jet production [53]. Exclusive W/Z+jets cross-sections for up to three jets are recently available at NLO precision [54, 59]. Higher order Monte Carlo generators apply a matching of the fi ed order QCD calculations to traditional parton shower models [55–58]. Thus, measurements of W/Z+jet fina states at the Tevatron are reasonably well described by the theoretical predictions [53, 59]. This gives confidenc that predictions for LHC energies can also be trusted at the percent level.

1.8 Standard Model Higgs Boson Production and Decay at the LHC

At the proton-proton collider LHC the Higgs boson is produced in several processes [10]:

- gluon fusion: $gg \to H$
- vector boson fusion: $qq \to qq + W^*W^*, Z^*Z^* \to qq + H$
- Higgs-strahlung off W or Z: $qq \to W, Z \to W, Z + H$
- Higgs bremsstrahlung off a top quark: $qq, gg \to t\bar{t} + H$

The corresponding Feynman diagrams are sketched in Fig. 1.12.

Gluon fusion is the by far dominating process with the highest cross-section over the whole Higgs mass range. Although the massless gluons do not couple directly to the Higgs, production via triangular quark loops is well possible. The large quark-mass coupling compensates the dynamic suppression due to the loop diagram. To

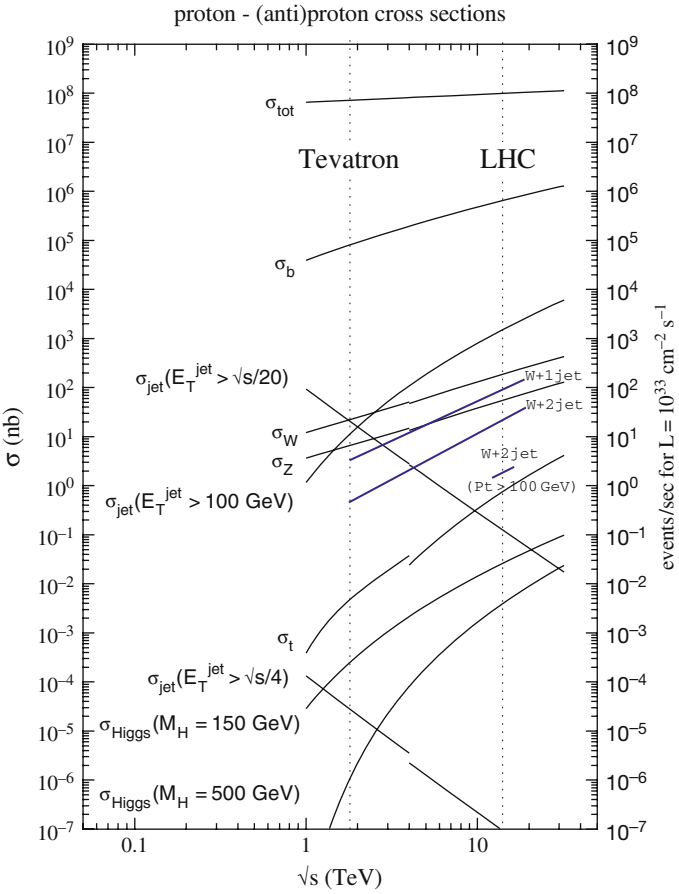

Fig. 1.11 Standard Model cross-sections at Tevatron and LHC energies, calculated at NLO precision. The discontinuities are due to the differences in parton content between $p\overline{p}$ and pp collisions. The *lines* indicated for W + 1,2 jets correspond to jets with $p_T > 20$ GeV and $|\eta| < 2.5$ [53]

lowest order the partonic $gg \to H$ cross-section can be written as [60]

$$\hat{\sigma}_{LO}(gg \to H) = \frac{\pi^2}{8M_{\mathrm{H}}}\Gamma_{LO}(H \to gg)\delta\left(\hat{s} - M_{\mathrm{H}}^2\right) \tag{1.109}$$

with

$$\Gamma_{LO}(H \to gg) = \frac{G_{\mathrm{F}}\alpha_s^2 M_{\mathrm{H}}^3}{36\sqrt{2}\pi^3}\left|\frac{3}{4}\sum_q A_q^H(\tau_q)\right|^2 . \tag{1.110}$$

The zero width approximation may be improved by substituting

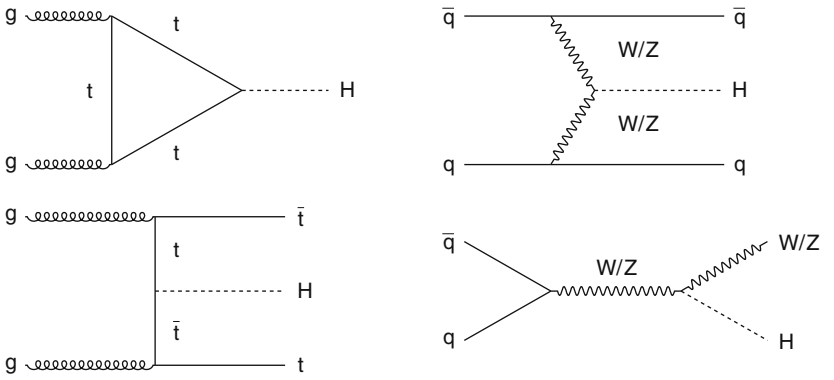

Fig. 1.12 Feynman diagrams for Higgs production showing gluon-gluon fusion and vector-boson fusion processes, as well as the associated Higgs production with top quarks and weak vector bosons

$$\delta\left(\hat{s} - M_{\mathrm{H}}^2\right) \;\rightarrow\; \frac{1}{\pi} \frac{\hat{s}\,\Gamma_{\mathrm{H}}/M_{\mathrm{H}}}{\left(\hat{s} - M_{\mathrm{H}}^2\right)^2 + (\hat{s}\,\Gamma_{\mathrm{H}}/M_{\mathrm{H}})^2} \tag{1.111}$$

The gluonic Higgs width $\Gamma_{LO}(H \rightarrow gg)$ is expressed in terms of form factors that depend on the squared Higgs-to-quark mass ratio $\tau_q = M_{\mathrm{H}}^2/4m_q^2$ [10]:

$$A_q^H(\tau_q) = \frac{2}{\tau_q^2}[\tau_q + (\tau_q - 1) f(\tau_q)] \tag{1.112}$$

$$f(\tau) = \begin{cases} \arcsin^2 \sqrt{\tau} & \tau \leq 1 \\ -\frac{1}{4}\left[\log \frac{1+\sqrt{1-\tau^{-1}}}{1-\sqrt{1-\tau^{-1}}} - i\pi\right]^2 & \tau > 1 \end{cases} \tag{1.113}$$

For small quark masses the form factor vanishes, and it approaches a value of $\frac{3}{4}$ for $m_q \gg M_{\mathrm{H}}$. This formula is also valid in extensions of the Standard Model, where higher mass fermions may appear in the loop and further increase the production cross-section. In the Standard Model, the main contribution is from the top quark loop. For Higgs masses below $2m_{\mathrm{t}}$ the infinit top mass approximation $m_{\mathrm{t}} \rightarrow \infty$ agrees with the full result within 10%, as can be seen in Fig. 1.13.

Corrections to the leading order cross-section are necessary because higher order QCD processes generally change the lowest order results significantl . For total cross-section calculations the corrections are usually phrased in terms of a K factor, which takes NLO or even higher order effects into account, e.g. $K = \sigma_{\mathrm{NLO}}/\sigma_{\mathrm{LO}}$ in case of NLO corrections. The LO cross-section can be written in the following form

$$\sigma(gg \rightarrow H) = \sigma_0^H \tau_H \frac{d\mathcal{L}^{gg}}{d\tau_H} \tag{1.114}$$

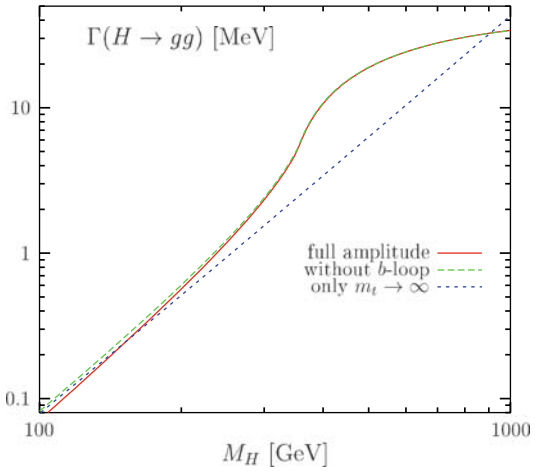

Fig. 1.13 Gluonic width of the Higgs boson including all quarks in the triangular loop, excluding the b-quark, and in the large m_t limit [10]

where $d\mathcal{L}^{gg}/d\tau_H$ denotes the gg luminosity of the pp collider as function of the Drell-Yann variable $\tau_H = M_H^2/s$, where s is the invariant collider energy squared. This notation is helpful when adding NLO terms, which arise through the real and virtual contributions, as shown in Fig. 1.14. The NLO cross-section is then given by:

$$\sigma(gg \to H) = \sigma_0^H \tau_H \left[1 + C^H \frac{\alpha_s}{\pi}\right] \frac{d\mathcal{L}^{gg}}{d\tau_H} + \Delta\sigma_{gg}^H + \Delta\sigma_{gq}^H + \Delta\sigma_{q\bar{q}}^H \qquad (1.115)$$

The coefficien C^H is the finit part of the virtual two-loop corrections [10], which are known to order α_s^5. The $\Delta\sigma$ terms are the hard contributions from gluon radiation in gg and gq scattering and $q\bar{q}$ annihilation. The corresponding K-factors for these terms are shown in Fig. 1.14. The virtual K_{virt} and the K_{gg} factors are the largest and in the order of 50%, while the others do not contribute much. The total correction at LHC energies is between 60 and 90% for low and high Higgs mass ranges, respectively.

Recent calculations even include NNLO, soft N^{3}LO and N^3 leading-log (N^{3}LL) calculations [61]. It turns out that NNLO corrections are still relatively large. Only at the following order the perturbation series starts to converge and yields smaller contributions (see Fig. 1.14). At all orders the dependence on the Higgs mass is large, and the gluon fusion cross-section at the LHC drops from about 60 pb for low M_{H} to below 10 pb for large M_{H}.

For the description of the transverse momentum, p_T, and rapidity, η, dependence of the $gg \to H$ process at higher orders Monte Carlo techniques are used. Furthermore, this allows the application of more realistic phase space cuts that are close to event selections applied on detector level. Calculations with the NNLO program FEHiP [62] have shown that NNLO effects can change the cross-section

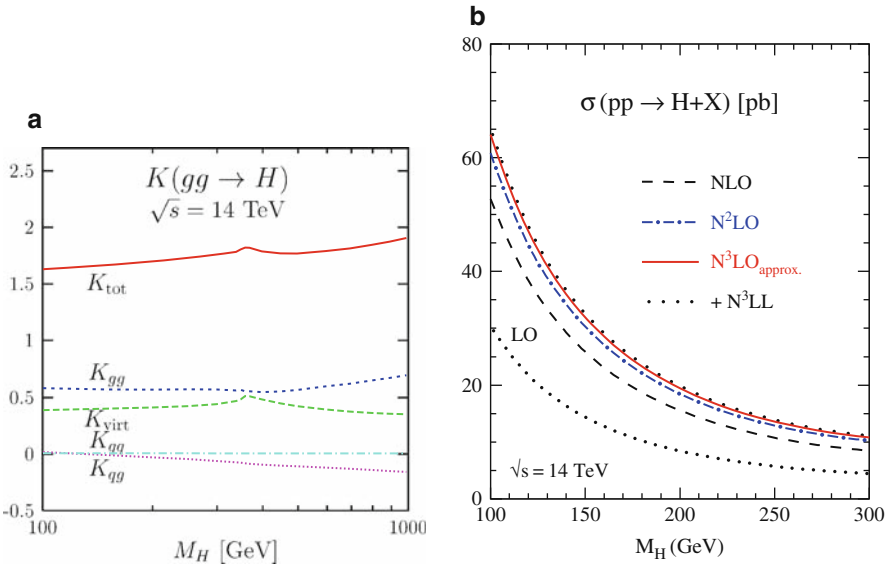

Fig. 1.14 (**a**) K-factors for the $gg \to H$ production cross-section at NLO [10]. (**b**) N^{3}LO calculations of the $gg \to H$ production cross-section [61]

within cuts by up to 5% [63]. Standard Monte Carlo programs like Pythia [64] or MC@NLO [58], only include LO or NLO effects, but may be improved to NNLO level by event reweighting [65].

Vector boson fusion (VBF) has a lower total cross-section than the gluon fusion process. But it provides the additional signature of quark jets with small transverse momentum, p_T, that can be identifie by the LHC detectors. In the longitudinal vector boson approximation [66] the total partonic cross-section is calculated to be [10]:

$$\hat{\sigma}_{LO}(qq \to qqH) = \frac{G_{\rm F}^3 M_V^4 N_c}{4\sqrt{2}\pi^3} C_V \left\{ \left(1 + \frac{M_{\rm H}^2}{\hat{s}}\right) \log \frac{\hat{s}}{M_{\rm H}^2} - 2 + 2\frac{M_{\rm H}^2}{\hat{s}} \right\} , \quad (1.116)$$

where $N_c = 3$ denotes the colour factor and M_V the vector boson mass. The factor C_V contains the quark-boson coupling constants:

$$C_Z = \left(\left(g_{\rm V}^{q1}\right)^2 + \left(g_{\rm A}^{q1}\right)^2 \right) \left(\left(g_{\rm V}^{q2}\right)^2 + \left(g_{\rm A}^{q2}\right)^2 \right) , \; C_W = 1 . \quad (1.117)$$

Because of the larger charged couplings the WW fusion is one order of magnitude larger than the ZZ fusion in this approximation. More complete calculations include all polarisations of the intermediate bosons, like the one displayed in Fig. 1.15, and NLO Monte Carlo programs are available [67].

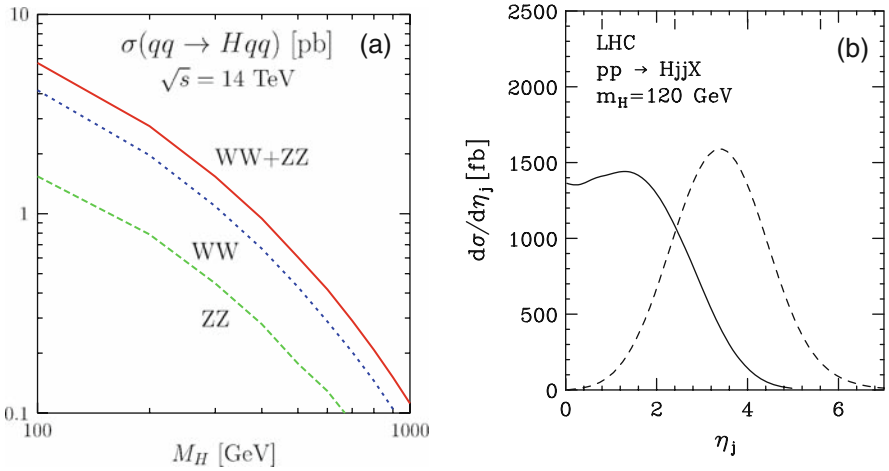

Fig. 1.15 (**a**) Vector boson fusion cross-section $\sigma(qq \to V^*V^* \to Hqq)$ at leading order [10]. (**b**) Pseudo-rapidity distributions of the quark jets in the VBF process. The most central jet is shown as a *solid line*, the most forward one as a *dashed line* [68]

Especially interesting is the kinematic behaviour of the quarks and bosons in the VBF process. The direction of the bosons emitted from the initial partons is in general close to the actual parton direction and their energies are of the order of the Higgs mass. Therefore the remaining parton quarks keep practically all their initial energy of about 1 TeV (at LHC) and have small transverse momentum, p_T. This also means that the hadronic quark jets are produced in the forward region. When expressed with the pseudo-rapidity, $\eta = -\log\tan\frac{\theta}{2}$, which is a function of the polar angle θ with respect to the colliding particles, values in the range $1 < \eta < 5$ are preferred, as illustrated in Fig. 1.15. Since there is no colour fl w between the two initial parton quarks a so-called rapidity gap is expected to be observed in VBF production, which means that the hadronic activity in the central η range is reduced. This feature is used to reduce background, mainly from $t\bar{t}$ events which are produced more centrally.

In the low Higgs mass region, $M_{\mathrm{H}} < 150$ GeV, also the associated production with W and Z bosons, $q\bar{q} \to WH, ZH$ has a sizable production rate. To lowest order the partonic cross-section is given by:

$$\hat{\sigma}(q\bar{q} \to VH) = \frac{G_{\mathrm{F}}^2 M_V^4}{72\pi\hat{s}} C_V \lambda^{1/2}\left(M_V^2, M_{\mathrm{H}}^2, \hat{s}\right) \frac{\lambda\left(M_V^2, M_{\mathrm{H}}^2, \hat{s}\right) + 12M_V^2/\hat{s}}{\left(1 - M_V^2/\hat{s}\right)^2} \tag{1.118}$$

with the coupling factors for $V = W, Z$:

$$C_Z = \left(g_{\mathrm{V}}^q\right)^2 + \left(g_{\mathrm{A}}^q\right)^2 \quad , \; C_W = 1 \tag{1.119}$$

and the two-body phase space function

$$\lambda(x, z, y) = \left(1 - \frac{x}{z} - \frac{y}{z}\right)^2 - 4\frac{xy}{z^2} \,. \tag{1.120}$$

Since it is a two-body decay the Higgs and the vector boson are produced back-to-back in the $q\bar{q}$ rest frame, which may be used in the search for the Higgs boson. The dependence of $\sigma(q\bar{q} \to VH)$ on the Higgs mass at the LHC is shown in Fig. 1.16, including NNLO QCD and electroweak radiative corrections.

The associated Higgs production with heavy quarks is like the associated vector boson production mainly important for low Higgs masses. There are ten leading order Feynman diagrams, since not only quark annihilation $q_1\bar{q}_1 \to g \to q_2\bar{q}_2 H$ contributes but also gluon fusion $gg \to q_2\bar{q}_2 H$ with s- and t-channel graphs. A closed expression is therefore quite involved. More details can be found in [10]. The evolution of $t\bar{t}H$ production with M_{H} for LO and NLO calculations is given in Fig. 1.16.

Figure 1.17 shows a summary of the different cross-sections for the various Higgs production mechanisms. At the LHC, gluon fusion clearly dominates and VBF is very important in all M_{H} ranges.

The decay of the Higgs boson eventually determines the search strategy at the LHC. The gluonic decay width already played a role in the gluon fusion process. However, due to the multi-hadronic environment caused by the underlying event and pile-up events, purely hadronic Higgs decays are very difficul to detect.

The other loop induced decay into two real photons, $H \to \gamma\gamma$, is more important because it has a clear detector signature. The decay width at lowest order is similar

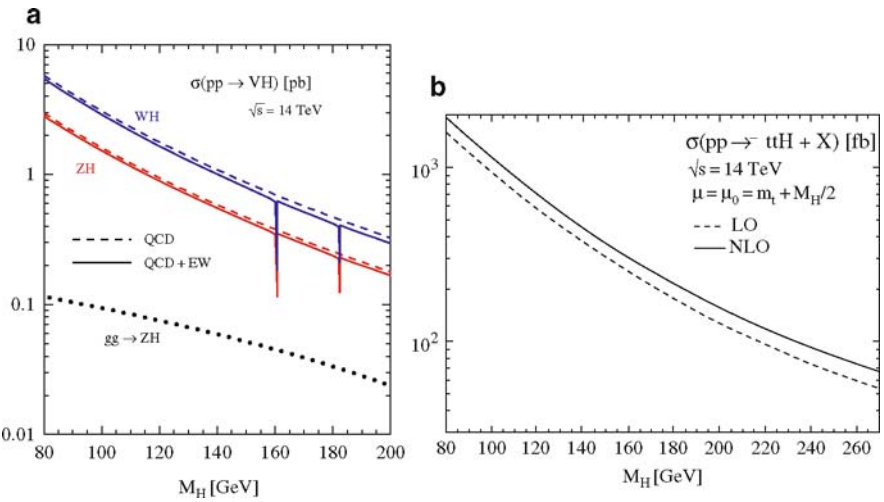

Fig. 1.16 (**a**) Higgs cross-sections for associated boson production. The *solid line* includes both NNLO QCD and electroweak radiative corrections, the *dashed line* only includes NNLO QCD effects. At this order of the perturbation series, also $gg \to ZH$ production contributes, which is indicated separately [69]. (**b**) Predictions of the $t\bar{t}H$ production at LHC energies at LO and NLO [70]

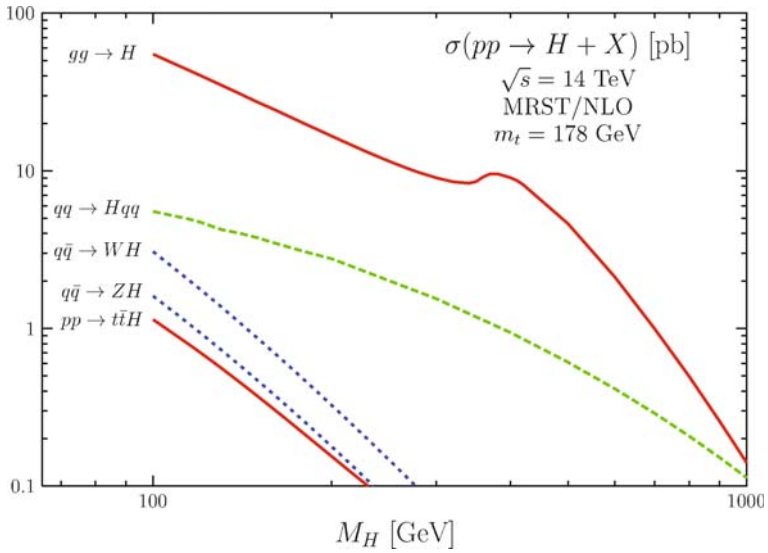

Fig. 1.17 Higgs production cross-sections at NLO [10]

to Eq. (1.110), except that the coupling to the fina state is electromagnetic and all charged particles are included in the loop:

$$\Gamma_{LO}(H \to \gamma\gamma) = \frac{G_{\mathrm{F}}\alpha_{\mathrm{QED}}^2 M_{\mathrm{H}}^3}{128\sqrt{2}\pi^3}\left|\sum_f N_c Q_f A_f^H(\tau_f) + A_W^H(\tau_W)\right|^2 \tag{1.121}$$

The additional term

$$A_W^H(\tau) = -\frac{1}{\tau^2}[2\tau^2 + 3\tau + 3(2\tau - 1)f(\tau)] \tag{1.122}$$

is from W bosons in the loop. The fermionic amplitude $A_f^H(\tau_f)$ and the functions $f(\tau)$ are define in Eq. (1.112). The colour factor, N_c, equals 3 for quarks and 1 for leptons.

The photonic decay width is much smaller than the gluonic one, as shown in Fig. 1.18. Both decrease fast with increasing Higgs mass when the decay channels to the heavy vector bosons open. This is also the case for the decay into low mass fermions.

The fermionic Higgs decay width at lowest order is given by

$$\Gamma(H \to f\bar{f}) = \frac{G_{\mathrm{F}} N_c}{4\sqrt{2}\pi} M_{\mathrm{H}} m_{\mathrm{f}}^2 \beta_f^3 \tag{1.123}$$

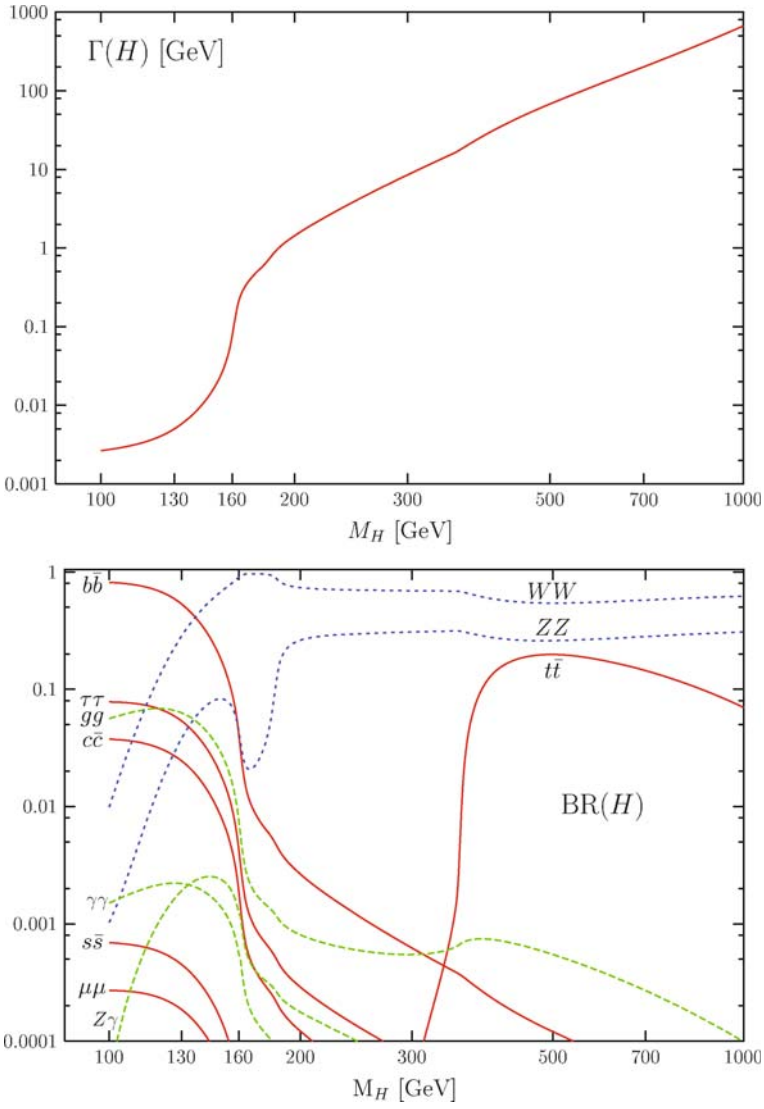

Fig. 1.18 Higgs total decay width (*top*) and branchings fractions (*bottom*). Two-loop QCD and leading electroweak corrections are included [10]

with the velocity of the fermions, $\beta_f = \sqrt{1 - 4m_f^2/M_H^2}$. Since the width is proportional to the fermion mass, mainly b and t quarks need to be considered. In this case, also QCD corrections need to be taken into account. If the Higgs mass is much larger than the quark mass, $M_H \gg m_q$, which is the case for the b quark, one can approximate at NLO:

$$\Gamma_{\mathrm{NLO}}(H \to q\bar{q}) \approx \frac{3G_{\mathrm{F}}}{4\sqrt{2}\pi} M_{\mathrm{H}} m_q^2 \left\{ 1 + \frac{4}{3}\frac{\alpha_s}{\pi}\left(\frac{9}{4} + \frac{3}{2}\log\frac{m_q^2}{M_{\mathrm{H}}^2} \right) \right\} \tag{1.124}$$

Also for the top quark, where the previous approximation does not hold any more, QCD corrections are formally added by a Δ_H^t term that depends on the top velocity β_t:

$$\Gamma_{\mathrm{NLO}}(H \to t\bar{t}) = \frac{3G_{\mathrm{F}}}{4\sqrt{2}\pi} M_{\mathrm{H}} m_{\mathrm{t}}^2 \beta_t^3 \left\{ 1 + \frac{4}{3}\frac{\alpha_s}{\pi}\Delta_H^t(\beta_t) \right\} \tag{1.125}$$

Due to the kinematics the branching fractions for low mass Higgs bosons, $M_{\mathrm{H}} < 150$ GeV, is dominated by the $b\bar{b}$ decay, as can be seen in Fig. 1.18. Also the decay to tau pairs is important. Top pairs are clearly only produced beyond the $2m_{\mathrm{t}}$ mass threshold. However, Higgs decays into vector boson pairs are still dominating the branching ratio in the high mass region $M_{\mathrm{H}} > 150$ GeV.

The Higgs partial decay width into two real vector bosons is given by

$$\Gamma(H \to VV) = \frac{G_{\mathrm{F}} M_{\mathrm{H}}^3}{16\sqrt{2}\pi} \delta_V \sqrt{1-4x}(1 - 4x + 12x^2) \tag{1.126}$$

with $\delta_W = 2$, $\delta_Z = 1$ and the mass ratio $x = \frac{M_V^2}{M_{\mathrm{H}}^2}$. This means that for very large Higgs masses the decay width into W bosons is two times larger than the one into Z bosons. Also interesting is the longitudinal polarisation fraction

$$\frac{\Gamma_L}{\Gamma_T + \Gamma_L} = \frac{1 - 4x + 4x^2}{1 - 4x + 12x^2} \tag{1.127}$$

which approaches 1 for large $M_{\mathrm{H}} \gg M_V$. The W and Z boson are therefore practically 100% longitudinally polarised in the high Higgs mass range.

When the Higgs mass is not large enough to decay into on-shell vector bosons, off-shell production needs to be taken into account, with the subsequent decay into lepton pairs, $H \to VV^* \to$ ffff. Details of this decay mode are described in Chap. 7.

The total Higgs decay width as a function of M_{H} is displayed in Fig. 1.18, together with the branching fractions into the various fina states.

1.9 Comparison of Theory and Experiment

Theories need to be compared with physics data to either approve or falsify their predictions. An important technique is the Monte Carlo modelling of physics processes, the subsequent simulation of their signatures in the experimental setup and the fina comparison to measured data distributions and interaction rates. Many Monte Carlo

generators are available and each has its specifi advantages and physics domains where they are applied.

Pythia [64] and Herwig [71] are multi-purpose generator and are used to simulate e^+e^-, ep, and hadron collision events. In collisions involving protons, the distribution of the partons inside the proton are taken from internal or external PDF libraries, like LHADPDF [72]. The most common PDF sets are CTEQ6 [73] and MRST [74] which are to be matched to the proper order of the QCD perturbation series of the Monte Carlo process. Pythia and Herwig (in combination with JIMMY [75]) also include the simulation of beam-remnants, underlying event and multiple interactions for pp and $p\bar{p}$ processes. Both programs are used for simulating the fragmentation and hadronisation of quarks and gluons and can be run together with other event generators.

At LEP, four-fermion fina states are mostly generated with the programs KandY [49], RacoonWW [48], GRC4f [76], EXCALIBUR [77], YFSZZ [78], and WPHACT [79]. Fermion-pair production is simulated with KORALZ [80] and its successor KK2f [81] and Bhabha scattering with BHWIDE [82] and TEEGG [83]. Hadronic 2-photon events are best described by PHOJET [84] and TWOGAM [85], while leptonic events of the same kind are usually generated with DIAG36 [86] and LEP4F [87]. Photon radiation off leptons can be produced with PHOTOS [88] and tau lepton decays are modelled in TAUOLA [89].

For proton-proton collisions at the LHC, the Sherpa [56] and Alpgen [57] programs implement parton-shower matching and are able to describe W/Z production with up to four and f ve jets, as well as VBF and b-quark associated Higgs production. Alpgen is applied in photon pair production, like the multi-purpose tool MadGraph/MadEvent [90], which also describes vector boson and vector boson pair production. The purpose of the AcerMC [91] package is the generation of $Zb\bar{b}/Zt\bar{t}$ as well as top pair events.

The MC@NLO [58] event generator is one of the few Monte Carlo tools including full NLO corrections to a selected set of processes in a consistent way, like inclusive W or Z production, $t\bar{t}$ production, electroweak boson pair production, as well as Higgs boson production and decay to W^+W^- and $\gamma\gamma$ fina states.

Production cross-sections of electroweak bosons at NNLO accuracy are available using FEWZ [92]. NLO calculations of the production of W and Z bosons and two jets with or without heavy quark tag can be performed with the MCFM [93] program and higher order corrections to $\gamma\gamma$ production are commonly done with RESBOS [94].

1.9.1 Hadronisation Models

There are three main Monte Carlo programs that are used for modelling fragmentation and hadronisation of quarks and gluons: Pythia [64], Herwig [71], and Ariadne [95]. The quarks and gluons are usually the result of the preceding Monte Carlo generation step.

In Pythia, the leading order hard scattering process is completed by the parton shower formalism to incorporate QED and QCD radiative leading-log corrections. In both initial- and final-state the showers develop according to the branchings $e \to e\gamma$, $q \to qg$, $q \to q\gamma$, $g \to gg$, and $g \to q\bar{q}$. The rates are proportional to the integral $\int P_{a\to bc}(z)\ , dz$, with the splitting kernel $P_{a\to bc}(z)$ which depends on the energy fraction $z = E_b/E_a$ carried by the splitting product b. The other particle has energy $(1 - z)$ after the splitting process. In the fina state, Pythia is evolving the showers from a virtuality scale scale $Q^2_{\max}$ down to a lower scale Q^2_0. Time ordering is done either according to the mass, m, of the shower partons or in recent Pythia versions according to p_T, where $p_T^2 = z(1 - z)m^2$.

The hadronisation package of Pythia can be used independently from the main generator. It applies the string fragmentation model to the parton shower products or to inputs from external generators. The string picture starts from the assumption that the energy between a colour dipole, like a $q\bar{q}$ pair for example, is linearly increasing with the distance between the charges. When the charges move further apart the energy stored in the string increases and it eventually breaks to form a new colour charge pair. A $q\bar{q}$ pair may split into two colour singlets $q\bar{q}'$ and $q'\bar{q}$. This process continues until only on-mass-shell hadrons remain. The subsequent decays of the hadrons are also treated by Pythia.

Several parameters are available to adjust the model to measured data. Especially the tuning of the parton shower and fragmentation are important, and in case of hadron collisions also the underlying event structure. For the parton showers the Lund fragmentation function is typically used for light, uds, fl vours and the Petersson function for heavy, c and b, fl vours with their tuned parameters. Furthermore, the Λ_{QCD} value used for the running of the strong coupling α_s in parton showers can be adjusted, as well as the parton shower cut-off value Q_0. In general, each experiment is individually trying to obtain the best description of the hadronic data distributions.

For LHC studies, the recent implementation of parton showering, commonly known as p_T-ordered showering, is used together with the new underlying event model where the phase-space is interleaved/shared between initial-state radiation (ISR) and the underlying event.

The Herwig program also treats quark fragmentation according to the parton shower model, fragmentation is however performed differently. In the Herwig cluster fragmentation model quarks and gluons from the parton showers combine locally into clusters. They are much less extended and less massive objects than strings. Only singlet combinations of partons are allowed to form clusters. These decay quasi isotropically into a small number of hadrons each. Like for Pythia, measured hadronic distributions are used to tune the Herwig model parameters, for example the QCD scale Λ_{QCD} or the cluster mass parameters which describe the cluster fission

The Ariadne program applies the dipole-cascade model to the fragmentation of quarks and gluons. The emission of a gluon g_1 from a quark anti-quark pair $q\bar{q}$ is modelled as radiation from a colour dipole between the q and the $\bar{q}$. The two new dipoles qg_1 and $g_1\bar{q}$ again radiate softer gluons. Radiation from the $q\bar{q}$ dipole is

suppressed by the colour factor $1/N_c^2$. The strong coupling α_s in the differential cross-sections $d\sigma/(dx\,dx_g)$ for the processes $q\bar{q} \to q\bar{q} + g$, $qg \to qg + g$, and $gg \to gg + g$ is evaluated at the transverse momentum scale, p_T^2, of the emission. The ordering of the gluon emission is also arranged according to the p_T^2 scale, where Sudakov form factors describe the probability of having emissions at a higher scale. Gluon splitting $g \to q\bar{q}$ is also possible and competes with the emission of another gluon. QED photon radiation in the cascade are treated similarly to the QCD gluon emission, however the photon emission is less probable since the electromagnetic coupling constant is much smaller than the strong coupling. Eventually, at the end of the cascade, the Pythia hadronisation model is applied to form the fina state hadrons. The main parameters that can be tuned in Ariadne to describe hadronic data are, for example, Λ_{QCD} and a p_t cut-off parameter.

1.9.2 Detector Simulation

The simulation of the interaction of the fina state particles with the detector is important to deduct the properties of the underlying physics processes from the measurement. The experiments at LEP and the Tevatron used the GEANT3 [96] FORTRAN program to calculate the particle trajectories and their energy depositions in the detector. Effects like ionisation energy loss, multiple scattering, electromagnetic showering and hadronic interaction with matter are implemented. The LHC experiments moved to the C++ coded GEANT4 [97] software, which is an evolution of GEANT3. The detailed detector simulations are in general very computing time consuming. Faster parameterisations [98] of the detector behaviour are therefore used in some applications under the condition that their precision is sufficien for the physics measurement.

References

1. S. L. Glashow, Nucl. Phys. **22** (1961) 579; S. Weinberg, Phys. Rev. Let. **19** (1967) 1264; A. Salam, *Elementary Particle Theory*, (ed) N. Svartholm, Stockholm, *Almquist and Wiksell*, 1968, p. 367; G. t'Hooft, Nucl. Phys. **B 35** (1971) 167; G. t'Hooft and M. Veltman, Nucl. Phys. **B 44** (1972) 189. 1, 4
2. H. Fritzsch, M. Gell-Mann and H. Leutwyler, Phys. Lett. **B 47** (1973) 365; H. D. Politzer, Phys. Rev. Let. **30** (1973) 1346; D. Gross and F. Wilczek, Phys. Rev. Let. **30** (1973) 1343; S. Weinberg, Phys. Rev. Let. **31** (1973) 494. 1
3. The Particle Data Group, C. Amsler, et al., Phys. Lett. **B 667** (2008) 1. 1, 6, 40
4. M. Kobayashi and T. Maskawa, Prog. Th. Phys. **49** 2 (1973) 652. 1
5. P. W. Higgs, Phys. Lett. **12** (1964) 132; *idem*, Phys. Rev. Lett. **13** (1964) 508; *idem*, Phys. Rev. **145** (1966) 1156; F. Englert and R. Brout, Phys. Rev. Lett. **13** (1964) 321; G. S. Guralnik, C. R. Hagne and T. W. B. Kibble, Phys. Rev. Lett **13** (1964) 585. 3, 7, 8, 15, 16
6. See for example: U. Dore and D. Orestano, Rep. Prog. Phys. **71** (2008) 106201; T. M. Raufer, *Neutrino Oscillation Results from MINOS and MiniBooNE*, arXiv:0808.0392v1; T. Schwetz, M. Tortola and J. W. F. Valle, New. J. Phys. **10** (2008) 113011, arXiv:0808.2016v2. 4

7. Z. Maki, M. Nakagawa and S. Sakata, Prog. Theor. Phys. **28** (1962) 870; B. Pontecorvo, Zh. Eksp. Teor. Fiz. **53** (1967) 1717. See [3] for a summary. 4
8. H. V. Klapdor-Kleingrothaus, et al., Mod. Phys. Lett. **A 16** (2001) 2409; C. E. Aalseth, et al., Mod. Phys. Lett. **A 17** (2002) 1475; H. V. Klapdor-Kleingrothaus and I. V. Krivosheina, Phys. Lett. **A 21** (2006) 1547; The latter reference claims evidence for a signal, which is however not fully accepted in the community and needs confirmatio by future experiments. A present status is e.g. reviewed in: A.S. Barabash, *Double beta decay: present status*,arXiv:0807.2948v1. 4
9. M. Chanowitz, *Strong WW scattering at the end of the 90's: theory and experimental prospects*, hep-ph/9812215v1. 7
10. For a review, see for example: Djouadi, A., *The Anatomy of Electro-Weak Symmetry Breaking. I: The Higgs boson in the Standard Model*, Phys. Rept. **457** (2008) 1, hep-ph/0503172; Djouadi, A., *The Anatomy of Electro-Weak Symmetry Breaking. II: The Higgs bosons in the Minimal Supersymmetric Model*, Phys. Rept. 459 (2008) 1, hep-ph/0503173. 7, 16, 27, 29, 30, 31, 32, 33, 34,
11. N. Cabibbo, L. Maiani, G. Parisi and R. Petronzio, Nucl. Phys. **B 158** (1979) 295; R. Dashen and H. Neuberger, Phys. Rev. Lett. **50** (1983) 1897; D. Callaway, Nucl. Phys. **B 233** (1984) 189; P. Hasenfratz and J. Nager, Z. Phys. **C 37** (1988) 477; J. Kuti, L. Lin, and Y. Shen, Phys. Rev. Lett. **61** (1988) 678; R. Chivukula and E. Simmons, Phys. Lett. **B 388** (1996) 788; U. M. Heller, M. Klomfass, H. Neuberger, P. Vranas, Nucl.Phys. **B 405** (1993) 555. 7
12. J. A. Casas, J. R. Espinosa and M. Quiros, Phys. Lett. **B 342** (1995) 171;Phys. Lett. **B 382** (1996) 374. 8
13. J. R. Espinosa, G. Giudice and A. Riotto, *Cosmological implications of the Higgs mass measurement*, arXiv:0710.2484v1. 8
14. T. Hambye and K. Riesselmann, Phys. Rev. **D 55** (1997) 7255; C. F. Kolda and H. Murayama, JHEP **0007** (2000) 035. 8
15. M. Veltman, Acta Phys. Pol. **B 12** (1981) 437. 9
16. see for example: A. Linde, *Inflationary Cosmology*, Lect. Notes Phys. **738** (2008) 1, arXiv:0705.0164v2. 9
17. F. Bezrukov and M. Shaposhnikov, *Standard Model Higgs boson mass from inflation: two loop analysis*, arXiv:0904.1537v. 9
18. S. Bethke, J.Phys. **G 26** R27, 2000; hep-ex/0004021. 10
19. CODATA Recommended Values of the Fundamental Physical Constants: P. J. Mohr, B. N. Taylor, and D. B. Newell, Rev. Mod. Phys. **80** (2008) 633. 11
20. M. Steinhauser, Phys. Lett **B 429** (1998) 158. 12
21. G. Montagna et al., Comp. Phys. Comm. **117** (1999) 278; A. B. Arbuzov et al., Comp. Phys. Comm. **174** (2006) 728. 12
22. H. Burkhardt and B. Pietrzyk, Phys. Rev. **D 72** (2005) 057501. 12
23. Tevatron Electroweak Working Group, for the CDF Collaboration, the DØ Collaboration, *Combination of CDF and D0 Results on the Mass of the Top Quark*, arXiv:0903.2503v1. 12, 13
24. F. Jegerlehner, *Renormalizing the Standard Model*, Preprint, PSI-PR-91-08, 1991. 13
25. The ALEPH, DELPHI, L3, OPAL, SLD Collaborations, the LEP Electroweak Working Group, the SLD Electroweak and Heavy Flavour Groups, Phys. Rep. **427** (2006) 257. 14
26. The ALEPH, DELPHI, L3, OPAL, SLC Collaborations, the LEP Electroweak Working Group, the Tevatron Electroweak Working Group, and the SLD electroweak and heavy fl vour groups, *Precision Electroweak Measurements and Constraints on the Standard Model*, CERN-PH-EP/2008-020; arXiv:0811.4682. Updates can be found at http://lepewwg.web.cern.ch/LEPEWWG/. 13, 14
27. The ALEPH, DELPHI, L3, OPAL Collaborations and the LEP Higgs Working Group, Phys. Lett. **B 565** (2003) 61. 14
28. R. Barbieri, S. Ferrara and C. A. Savoy, Phys. Lett. **B 119** (1982) 343; A. H. Chamseddine, R. Arnowitt and P. Nath, Phys. Rev. Lett. **49** (1982) 970; L. Hall, J. Lykken and S. Weinberg, Phys. Rev. **D 27** (1983) 2359; P. Nath, R. Arnowitt and A. H .Chamseddine, Nucl. Phys. **B 227** (1983) 121; P. Nath, R. Arnowitt and A. H. Chamseddine, *Applied N=1 Supergravity*

Trieste lecture series, vol. I, World Scientific 1984; H. P. Nilles, *Supersymmetry, Supergravity and Particle Physics*, Phys. Rep. **110** (1984) 1. 15
29. P. Fayet, Phys. Lett. **B 70** (1977) 461; Phys. Lett. **B 86** (1979) 272; Phys. Lett. **B 175** (1986) 471; M. Dine, A. E. Nelson, Y. Nir and Y. Shirman, Phys. Rev. **D 53** (1996) 2658; H. Baer, M. Brhlik, C. H. Chen and X. Tata, Phys. Rev. **D 55** (1997) 4463; H. Baer, P. G. Mercadante, X. Tata and Y. L. Wang, Phys. Rev. **D 60** (1999) 055001; S. Dimopoulos, S. Thomas and J. D. Wells, Nucl. Phys. **B 488** (1997) 39; J. R. Ellis, J. L. Lopez and D. V. Nanopoulos, Phys. Lett. **B 394** (1997) 354; and the review: G.F. Giudice, R. Rattazzi, *Theories with Gauge-Mediated Supersymmetry Breaking*, Phys. Rep. **322** (1999) 419, hep-ph/9801271v2. 15
30. The ATLAS Collaboration, G. Aad, et al., *Expected Performance of the ATLAS Experiment Detector, Trigger, Physics*, CERN-OPEN-2008-020, arXiv:0901.0512. 15, 16
31. W. Beenakker, R. Hopker, M. Spira and P. M. Zerwas, Nucl. Phys. **B 492** (1997) 51; W. Beenakker, et al., Phys. Rev. Lett. **83** (1999) 3780; Prospino2, http://www.ph.ed.ac.uk/tplehn/prospino/. 15
32. The ATLAS Collaboration, *Detector and Physics Performance Technical Design Report*, CERN/LHCC/99-14/15, 1999. 16
33. B. C. Allanach, A. Djouadi, J. L. Kneur, W. Porod and P. Slavich, JHEP **0409** (2004) 044. 15
34. The CMS Collaboration, G. L. Bayatian, et al., CMS Physics Technical Design Report, Vol. II: Physics Performance, CERN/LHCC 2006-021. 16
35. see for example: M. Drees, R. Godbole and P. Roy, *Theory and Phenomenology of Sparticles*, World Scientifi Publishing Company, 2004. 16
36. M. C. Chen, S. Dawson, C. B. Jackson, Phys. Rev. **D 78** (2008) 093001; A. Aranda, J. Hernandez-Sanchez, P. Q. Hung, *Implications of the discovery of a Higgs triplet on electroweak right-handed neutrinos*, arXiv:0809.2791v1; E. Ma, U. Sarkar, Phys. Rev. Lett. **80** (1998) 5716. 17
37. M. Gell-Mann, P. Ramond and R. Slansky, in Supergravity, (ed) by D. Freedman et al., North Holland (1979); T. Yanagida, Prog. Theor. Phys. **64** (1980) 1103. 17
38. M. Aoki and S. Kanemura, Phys. Rev. **D 77** (2008) 095009. 17
39. The DØ Collaboration, V. Abazov, et al., Phys. Rev. Lett. **101** (2008) 071803, and references therein. 17
40. M. Schmaltz and D. Tucker-Smith, Ann. Rev. Nucl. Part. Sci. **55** (2005) 229. 17
41. H. C. Cheng, *Little Higgs, Non-standard Higgs, No Higgs and All That*, arXiv:0710.3407v1. 17
42. see for example: C. T. Hill, E. H. Simmons, Phys. Rep. **381** (2003) 235; Erratum ibid. **390** (2004) 553. 17
43. C. Csaki, C. Grojean, L. Pilo and J. Terning, Phys. Rev. Lett. **92** (2004) 101802; C. Englert, B. Jager, M. Worek and D. Zeppenfeld, *Observing Strongly Interacting Vector Boson Systems at the CERN Large Hadron Collider*, arXiv:0810.4861v1. 17
44. A. Alboteanu, W. Kilian and J. Reuter, JHEP **0811** (2008) 010. 17
45. The ALEPH Collaboration, the DELPHI Collaboration, the L3 Collaboration, the OPAL Collaboration, the SLD Collaboration, the LEP Electroweak Working Group, the SLD electroweak, heavy fl vour groups, Phys. Rept. **427** (2006) 257; hep-ex/0509008v3. 17, 18
46. G. Altarelli,. T. Sjostrand and F. Zwirner, (eds), *Workshop on Physics at LEP2*, Yellow report CERN 96-01, 1996. 23
47. GENTLE version 2.0 is used. D. Bardin et al., Comp. Phys. Comm. **104** (1997) 161. 24
48. RacoonWW, A. Denner, S. Dittmaier, M. Roth and D. Wackeroth, Phys. Lett. **B 475** (2000) 127; A.Denner, S.Dittmaier, M. Roth and D.Wackeroth, *W-pair production at future e+e-colliders: precise predictions from RACOONWW*, hep-ph/9912447. 25, 37, 41
49. KandY runs concurrently KORALW version 1.51 and YFSWW3 version 1.16. S. Jadach et al., Comp. Phys. Comm. **140** (2001) 475. 25, 37, 41
50. see [48] and [49]. 25
51. M. Beneke, et al., *Four-fermion production near the W pair production threshold*, CERN-PH-TH-07-107, arXiv:0707.0773v1 [hep-ph]. 25
52. M. Dittmar, F. Pauss and D. Zürcher, Phys. Rev. **D 56** (1997) 7284. 26, 27

53. J. M. Campbell, *Overview of the theory of W/Z + jets and heavy flavor*, arXiv:0808.3517v1, and references therein. 27, 28
54. C. F. Berger, Z. Bern, L. J. Dixon, F. Febres Cordero, D. Forde, H. Ita, D. A. Kosower and D. Maitre, *One-Loop Multi-Parton Amplitudes with a Vector Boson for the LHC*, arXiv:0808.0941v1. 27
55. S. Catani, F. Krauss, R. Kuhn and B. R. Webber, JHEP **0111** (2001) 063.; M. L. Mangano, M. Moretti, F. Piccinini, R. Pittau and A. D. Polosa, JHEP **0307** (2003) 001; S. Frixione, P. Nason and B. R. Webber, JHEP **0308** (2003) 007. 27
56. T. Gleisberg, S. Hoeche, F. Krauss, A. Schaelicke, S. Schumann and J. Winter, JHEP **0402** (2004) 056. 27, 37
57. M. L. Mangano, M. Moretti, F. Piccinini, R. Pittau and A. Polosa, JHEP **0307** (2003) 001; F. Caravaglios, M. L. Mangano, M. Moretti and R. Pittau, Nucl.Phys. **B 539** (1999) 232. 27, 37
58. St. Frixione, et al., JHEP **06**(2002)029 . 27, 31, 37
59. C. F. Berger, Z. Bern, L. J. Dixon, F. Febres Cordero, D. Forde, T. Gleisberg, H. Ita, D. A. Kosower and D. Maître, *Next-to-Leading Order QCD Predictions for W +3-Jet Distributions at Hadron Colliders*, arXiv:0907.1984; Phys. Rev. Lett. **102** (2009) 222001, arXiv:0902.2760; 27
60. M. Spira and P. M. Zerwas, Lect. Notes Phys. **512** (1998) 161, hep-ph/9803257v2. 28
61. S. Moch and A. Vogt, Phys. Lett. **B 631** (2005) 48. 30, 31
62. Ch. Anastasiou, K. Melnikov and F. Petriello, Nucl. Phys. **B 724** (2005) 197. 30
63. R. Harlander, Pramana **67** (2006) 875; hep-ph/0606095v1. 31
64. T. Sjöstrand, P. Edén, C. Friberg, L. Lönnblad, G. Miu, S. Mrenna and E. Norrbin, Comp. Phys. Comm. **135** (2001) 238; For colour reconnection and Bose-Einstein correlation studies PYTHIA version 6.121 is used. T. Sjöstrand, *Recent Progress in PYTHIA*, Preprint, LU-TP-99-42, hep-ph/0001032. 31, 37
65. G. Davatz, et al., JHEP **07** (2006) 037. 31
66. R. M. Godbole and S. D. Rindani, Z. Phys. **C 36** (1987) 395. 31
67. K. Arnold, et al., KA-TP-31-2008, SFB/CPP-08-95, arXiv:0811.4559v2. 31
68. D. Zeppenfeld, *Collider Physics*, hep-ph/9902307. 32
69. O. Brein, M. L. Ciccolini, S. Dittmaier, A. Djouadi, M. Krämer and R. Harlander, hep-ph/0402003. 33
70. W. Beenakker, S. Dittmaier, M. Krämer, B. Plümper, M. Spira and P. M. Zerwas, Phys. Rev. Lett. **87** (2001) 201805; ibid. Nucl. Phys. **B 653** (2003) 151. 33
71. G. Corcella, I. G. Knowles, G. Marchesini, S. Moretti, K. Odagiri, P. Richardson, M. H. Seymour and B. R. Webber, JHEP **0101** (2001) 010; hep-ph/0210213. 37
72. LHADPDF, http://hepforge.cedar.ac.uk/lhapdf/; M. R. Whalley, D. Bourilkov, R. C. Group, hep-ph/0508110. 37
73. J. Pumplin, D. R. Stump, J. Huston, H. L. Lai, P. Nadolsky and W. K. Tung, JHEP **0207** (2002) 012, hep-ph/0201195; J. Pumplin, et al., *Parton Distributions and the Strong Coupling Strength: CTEQ6AB PDFs*, hep-ph/0512167. 37
74. A. D. Martin, W. J. Stirling, R. S. Thorne and G. Watt, *Update of Parton Distributions at NNLO*, arXiv:0706.0459v3. 37
75. J. M. Butterworth, J. R. Forshaw and M. H. Seymour *Multiparton Interactions in Photoproduction at HERA*, CERN-TH/95-82, MC-TH-96/05, UCL-HEP 96-02, hep-ph/9601371, Z. Phys. **C 72** (1996) 637; L. Lönnblad, M. Seymour, et al., *gamma-gamma Event Generators*, hep-ph/9512371; J. M. Butterworth and J. R. Forshaw, *Photoproduction of Multi-Jet Events at HERA - A Monte Carlo Simulation*, J.Phys. **G 19** (1993) 1657. 37
76. J. Fujimoto, et al., Comp. Phys. Comm. **100** (1997) 128; hep-ph/9605312. 37
77. F. A. Berends, R. Kleiss and R. Pittau, Nucl. Phys. **B 424** (1994) 308; Nucl. Phys. **B 426** (1994) 344; Nucl. Phys. (Proc. Suppl.) **B 37** (1994) 163; R. Kleiss and R. Pittau, Comp. Phys. Comm. **83** (1994) 141; R. Pittau, Phys. Lett. **B 335** (1994) 490. 37
78. S. Jadach, W. Placzek and B. F. L. Ward, Phys. Rev. **D 56** (1997) 6939. 37

79. E. Accomando, A. Ballestrero, E. Maina, Comput. Phys. Commun. **150** (2003) 166; hep-ph/0204052. 37
80. S. Jadach, B. F. L. Ward and Z. Wąs, Comp. Phys. Comm. **79** (1994) 503. 37
81. S. Jadach, B. F. L. Ward and Z. Wąs, *The precision Monte Carlo event generator KK for two-fermion final states in* e^+e^- *collisions*, CERN-TH/99-235. 37
82. S. Jadach, W. Placzek, B. F. L. Ward, Phys. Lett. **B 390** (1997) 298–308. 37
83. D. Karlen, Nucl. Phys. **B 289** (1987) 23. 37
84. R. Engel, Z. Phys. **C 66** (1995) 203; R. Engel and J. Ranft, Phys. Rev. **D 54** (1996) 4244. 37
85. S. Nova, A. Olshevski and T. Todorov, *MONTE-CARLO Event Generator for two Photon Physics*, DELPHI internal note 90-35, 1990. 37
86. F. A. Berends, P. H. Daverfeldt and R. Kleiss, Nucl. Phys. **B 253** (1985) 441. 37
87. J. A. M. Vermaseren, J. Smith and G. Grammer Jr, Phys. Rev. **D 19** (1979) 137; J. A. M. Vermaseren, Nucl. Phys. **B 229** (1983) 347. 37
88. E. Barberio and Z. Wąs, Comp. Phys. Comm. **79** (1994) 291. 37
89. Z. Was, Nucl. Phys. Proc. Suppl. **98** (2001) 96. 37
90. J. Alwall, et al., JHEP **09** (2007) 028. 37
91. B. P. Kersevan, E. Richter-Was, *The Monte Carlo Event Generator AcerMC version 3.4*, TPJU-6/2004, hep-ph/0405247. 37
92. K. Melnikov and F. Petriello, Phys. Rev. Lett. **96** (2006) 231803. 37
93. J. Campbell and R. K. Ellis, User Guide available at http://mcfm.fnal.gov/ (2007); J. Campbell, R. K. Ellis, G. Zanderighi, JHEP **0610** (2006) 028; J. Campbell, R. K. Ellis, F. Maltoni, S. Willenbrock, Phys. Rev. **D 73** (2006) 054007; J. Campbell, R. K. Ellis, F. Maltoni, S. Willenbrock, Phys. Rev. **D 75** (2007) 054015. 37
94. C. Balazs, E. Berger, P. Nadolsky and C. -P. Yuan, Phys. Lett. **B 637** (2006) 235. 37
95. L. Lönnblad, Comp. Phys. Comm. **71** (1992) 15. 37
96. See R. Brun et al, *GEANT 3*, CERN DD/EE/84-1 (Revised), September 1987; The GHEISHA program (H. Fesefeldt, RWTH Aachen Report PITHA 85/02, 1985) is used to simulate hadronic interactions. 39
97. S. Agostinelli, et al., Nucl. Inst. Meth. **A 506** (2003) 250; J. Allison, et al., IEEE Trans. Nucl. Sci. **53** (2006) 270. 39
98. Fast detector simulations are for example developed for the ATLAS detector: K. Mahboubi and K. Jakobs, *A fast parameterization of electromagnetic and hadronic calorimeter showers*, ATLAS Public Note ATL-SOFT-PUB-2006-001; D. Cavalli, et al., *Performance of the ATLAS fast simulation ATLFAST* ATLAS Internal Notes ATL-PHYS-INT-2007-005, ATL-COM-PHYS-2007-012; E. Barberio and A. Straessner, *Parameterization of electromagnetic showers for the ATLAS detector*, ATLAS Note ATL-COM-PHYS-2004-015. 39